MOX-Report No. 52/2023

A space-time discontinuous Galerkin method for coupled poroelasticity-elasticity problems

Antonietti, P.F.; Botti, M.; Mazzieri, I.

A SPACE-TIME DISCONTINUOUS GALERKIN METHOD FOR COUPLED POROELASTICITY-ELASTICITY PROBLEMS

PAOLA F. ANTONIETTI*, MICHELE BOTTI†, AND ILARIO MAZZIERI†

Abstract. This work is concerned with the analysis of a space-time finite element discontinuous Galerkin method on polytopal meshes (XT-PolydG) for the numerical discretization of wave propagation in coupled poroelastic-elastic media. The mathematical model consists of the low-frequency Biot's equations in the poroelastic medium and the elastodynamics equation for the elastic one. To realize the coupling, suitable transmission conditions on the interface between the two domains are (weakly) embedded in the formulation. The proposed PolydG discretization in space is then coupled with a dG time integration scheme, resulting in a full space-time dG discretization. We present the stability analysis for both the continuous and the semidiscrete formulations, and we derive error estimates for the semidiscrete formulation in a suitable energy norm. The method is applied to a wide set of numerical test cases to verify the theoretical bounds. Examples of physical interest are also presented to investigate the capability of the proposed method in relevant geophysical scenarios.

Key words. poroelasticity; multiphysics; space-time discontinuous Galerkin methods; polygonal and polyhedral meshes; stability and convergence analysis

AMS subject classifications. 65M12, 65M60

1. Introduction. The numerical simulation of wave propagation in heterogeneous media is an important aspect of a wide range of scientific problems including acoustic engineering [73], vibro-acoustics [54], aeronautical engineering [32], biomedical engineering [48], computational seismology [31], and oil and gas exploration [80, 59]. In this framework, recent studies have been concerned with the propagation of seismic waves in coupled elastic and poroelastic media. For the region of reservoirs, Biot's model of poroelastic wave equations is selected while for the background region [22], the visco-elastic wave equation is employed, cf. [60]. Poroelastic-elastic problems model elastic waves impacting a porous material and consequently propagating through it. The coupling between the elastic and the poroelastic domain is a more general realization of the physically consistent transmission conditions discussed in [47, 60, 75]. Indeed, in our case, partial filtration at the interface can be also taken into account. Based on a second-order in-time displacement formulation, in this paper, we present a high-order space-time discontinuous Galerkin method on polytopal grids (XT-PolydG) for the discretization of a coupled poroelastic-elastic problem. The theory developed completes the one presented in [9] and [5], where coupled poroelastic-acoustic and elastic-acoustic problems were studied, respectively. We remark that the geometric flexibility, due to mild regularity requirements on the underlying polytopal mesh, together with the arbitrary-order accuracy featured by the proposed XT-PolydG method is fundamental within the applicative context under investigation as it guarantees: (i) *flexibility* in the representation of the geometry; (ii) high level of *accuracy* in both space and time dimensions; (iii) *efficiency* for parallel computation. Finally, the coupling conditions between the elastic and the poroelastic domains are naturally incorporated (in a weak sense) in the proposed scheme.

In the literature, we can find many works concerning the numerical discretization of coupled poroelastic models. Here, we recall, e.g., the semi-analytical solution and the plane wave decomposition method [55, 63], the Lagrange Multipliers method [67, 3, 43], the finite and boundary element methods [21, 42, 41], mixed and dis-

---
*MOX, Dipartimento di Matematica, Politecnico di Milano, Italy. (paola.antonietti@polimi.it, michele.botti@polimi.it, ilario.mazzieri@polimi.it).

continuous finite elements [20, 65, 45, 4], the spectral and pseudo-spectral element method [60, 68], the finite difference method, [35, 77, 57, 79], the ADER scheme [76, 36, 33, 78, 81, 39], the virtual element method [24], and the references therein. Here, by taking inspiration from [45], we analyze an Interior Penalty discontinuous Galerkin formulation of the coupled problem, where the interface conditions are naturally taken into account by the penalization terms. The geometrical flexibility and high-order accuracy of the proposed scheme are ensured by the use of polygonal meshes and by the dG discretization in the time dimension. We refer the reader to [52, 37, 50, 44] for early results on time dG schemes for wave type equations, to [74, 1, 38] for first-order hyperbolic problems, to [53, 18] and to [46, 58, 64] for Trefftz and tent-pitching techniques, to [17, 11, 14] for the second-order wave equation, and to [61] for a comprehensive review. On the other hand, regarding polytopal dG methods, we refer the reader to [10, 19, 12, 28, 34, 26, 27] for early results on elliptic and parabolic problems, to [13, 15] for linear and non-linear hyperbolic problems, and to [5, 6, 9, 8] for coupled wave propagation problems. A dG approximation of the fully coupled thermo-poroelastic problem is presented in [7]. Wave propagation in thermo-poroelastic media with dG methods is discussed in [23].

The remaining part of the paper is structured as follows. In Section 2 we present the coupled poroelastic-elastic differential model for wave propagation in heterogeneous media, we discuss the weak formulation and present the stability analysis in the continuous setting. In Section 3 we introduce the polytopal discontinuous Galerkin space discretization and analyze its stability. The convergence analysis of the aforementioned discretization is discussed in Section 4, while a dG time integration scheme and its algebraic formulation are presented in Section 5. Section 6 contains verification test cases to validate the theoretical error bounds as well as numerical tests of physical interest. Finally, in Section 8 we draw some conclusions and discuss some perspectives about future work.

Notation. Let $\Omega \subset \mathbb{R}^d$, $d = 2, 3$, be an open, convex polygonal/polyhedral domain with Lipschitz boundary $\partial\Omega$. In what follows, for $X \subseteq \Omega$, the notation $\boldsymbol{L}^2(X)$ is adopted in place of $[L^2(X)]^d$, with $d \in \{2, 3\}$. The scalar product in $L^2(X)$ is denoted by $(\cdot, \cdot)_X$, with associated norm $\|\cdot\|_X$. Similarly, $\boldsymbol{H}^\ell(X)$ is defined as $[H^\ell(X)]^d$, with $\ell \geq 0$, equipped with the norm $\|\cdot\|_{\ell,X}$, assuming conventionally that $\boldsymbol{H}^0(X) \equiv \boldsymbol{L}^2(X)$. In addition, we will use $\boldsymbol{H}(\mathrm{div}, X)$ to denote the space of $\boldsymbol{L}^2(X)$ functions with square integrable divergence. For a given final time $T > 0$, $k \in \mathbb{N}$, and a Hilbert space H, the usual notation $C^k([0, T]; H)$ is adopted for the space of H-valued functions, k-times continuously differentiable in $[0, T]$. The notation $x \lesssim y$ stands for $x \leq Cy$, with $C > 0$, independent of the discretization parameters, but possibly dependent on the physical coefficients and the final time T.

2. The physical model and governing equations. The computational domain Ω can be seen as the union of two disjoint, polygonal/polyhedral regions: $\Omega = \Omega_e \cup \Omega_p$, representing the elastic and the poroelastic domains, respectively. The two subdomains share part of their boundary, resulting in the Lipschitz-regular interface $\Gamma_I = \partial\Omega_e \cap \partial\Omega_p$, being $\partial\Omega_e$ and $\partial\Omega_p$ the boundaries of elastic and poroelastic domains, respectively. See Figure 1. We set $\Gamma_e = \partial\Omega_e \setminus \Gamma_I$ and $\Gamma_p = \partial\Omega_p \setminus \Gamma_I$, so that $\Gamma_i \cap \Gamma_I = \emptyset$ for $i = \{e, p\}$. For the sake of presentation, on Γ_i, $i = \{e, p\}$ we apply homogeneous Dirichlet conditions. The general case follows similarly. Additionally, we suppose that the Hausdorff measures of Γ_e, Γ_p, and Γ_I are strictly positive, but the following theory also covers the cases: *i)* $\Omega_p = \Gamma_I = \emptyset$, i.e. $\Omega \equiv \Omega_e$ and *ii)*
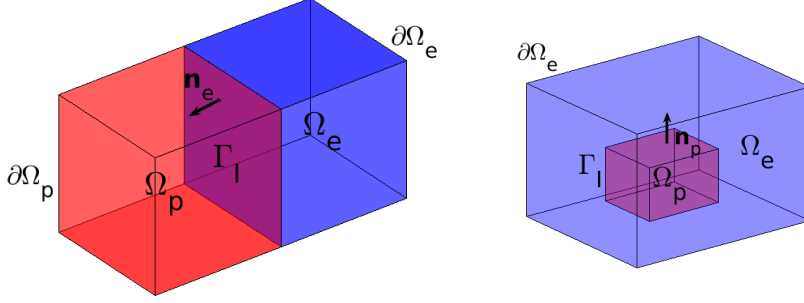
Fig. 1: Simplified representations of the domain $\Omega = \Omega_p \cup \Omega_e$. Here, $\Gamma_I = \partial\Omega_e \cap \partial\Omega_p$ represents the interface bewteen the elastic and the poroelastic domains, where $\partial\Omega_e$ and $\partial\Omega_p$ are the boundaries of elastic and poroelastic sub-domains, respectively.

$\Omega_e = \Gamma_I = \emptyset$, i.e. $\Omega \equiv \Omega_p$; as well as *iii)* $\partial\Omega_p = \Gamma_I$, i.e. $\Gamma_p = \emptyset$ and *iv)* $\partial\Omega_e = \Gamma_I$, i.e. $\Gamma_e = \emptyset$. The outer unit normal vectors to $\partial\Omega_e$ and $\partial\Omega_p$ are denoted by $\boldsymbol{n}_e$, and $\boldsymbol{n}_p$ respectively, so that $\boldsymbol{n}_p = -\boldsymbol{n}_e$ on Γ_I.

Elastic domain. In the solid elastic domain Ω_e, we consider the linear visco-elastodynamics model

$$(2.1) \qquad \rho_e \ddot{\boldsymbol{u}}_e + 2\rho_e \zeta \dot{\boldsymbol{u}}_e + \rho_e \zeta^2 \boldsymbol{u}_e - \nabla \cdot \boldsymbol{\sigma}_e(\boldsymbol{u}_e) = \boldsymbol{f}_e, \quad \text{in } \Omega_e \times (0, T],$$

where $\boldsymbol{u}_e$ represents the solid displacement, $\rho_e > 0$ is the medium density, $\zeta > 0$ is an attenuation parameter [8], and $\boldsymbol{f}_e$ is a given external load. The stress tensor $\boldsymbol{\sigma}_e(\boldsymbol{u})$ is defined as $\boldsymbol{\sigma}_e(\boldsymbol{u}) = \mathbb{C} : \boldsymbol{\epsilon}(\boldsymbol{u})$, where $\boldsymbol{\epsilon}(\boldsymbol{u}) = \frac{1}{2}(\nabla\boldsymbol{u} + \nabla\boldsymbol{u}^T)$ is the strain tensor, and $\mathbb{C}$ is the fourth-order, symmetric and uniformly elliptic elasticity tensor defined by

$$\mathbb{C} : \boldsymbol{\tau} = 2\mu\boldsymbol{\tau} + \lambda \text{tr}(\boldsymbol{\tau}) \qquad \text{for all } \boldsymbol{\tau} \in \mathbb{R}^{d \times d},$$

with $\text{tr}(\boldsymbol{\tau}) = \sum_{i=1}^d \boldsymbol{\tau}_{ii}$. Here, $\lambda \geq 0$ and $\mu \geq \mu_0 > 0$ are the Lamé coefficients.

Poroelastic domain. In the poroelastic domain Ω_p, following [9], we consider the low-frequency Biot's equations:

$$(2.2) \quad \begin{cases} \rho_p \ddot{\boldsymbol{u}}_p + \rho_f \ddot{\boldsymbol{u}}_f + 2\rho_p \zeta \dot{\boldsymbol{u}}_p + \rho_p \zeta^2 \boldsymbol{u}_p - \nabla \cdot \boldsymbol{\sigma}_p(\boldsymbol{u}_p, \boldsymbol{u}_f) = \boldsymbol{f}_p, & \text{in } \Omega_p \times (0, T], \\ \rho_f \ddot{\boldsymbol{u}}_p + \rho_w \ddot{\boldsymbol{u}}_f + \frac{\eta}{k} \dot{\boldsymbol{u}}_f + \nabla p(\boldsymbol{u}_p, \boldsymbol{u}_f) = \boldsymbol{g}_p, & \text{in } \Omega_p \times (0, T]. \end{cases}$$

Here, $\boldsymbol{u}_p$ and $\boldsymbol{u}_f$ represent the solid and filtration displacements, respectively. In (2.2) the average density ρ_p is given by $\rho_p = \phi\rho_f + (1 - \phi)\rho_s$, where $\rho_s > 0$ is the solid density, $\rho_f > 0$ is the saturating fluid density, ρ_w is defined as $\rho_w = \frac{a}{\phi}\rho_f$, being ϕ the *porosity* satisfying $0 < \phi_0 \leq \phi \leq \phi_1 < 1$, and being $a > 1$ the *tortuosity* measuring the deviation of the fluid paths from straight streamlines, cf. [70]. The dynamic *viscosity* of the fluid is represented by $\eta > 0$ while the absolute *permeability* by $k > 0$. In (2.2), $\mathbf{f}_p$ and $\mathbf{g}_p$ are given (regular enough) loading and source terms, respectively. In Ω_p, we assume the following constitutive laws, cf. [40], for the stress $\boldsymbol{\sigma}_p$ and pressure p:

$$(2.3) \quad \boldsymbol{\sigma}_p(\boldsymbol{u}_p, \boldsymbol{u}_f) = \boldsymbol{\sigma}_e(\boldsymbol{u}_p) - \beta \, p(\boldsymbol{u}_p, \boldsymbol{u}_f)\boldsymbol{I}, \quad p(\boldsymbol{u}_p, \boldsymbol{u}_f) = -m(\beta \nabla \cdot \boldsymbol{u}_p + \nabla \cdot \boldsymbol{u}_f),$$

where the Biot–Willis's coefficient β and the Biot's modulus m are such that $\phi < \beta \leq 1$ and $m \geq m_0 > 0$. It can be shown that the dilatation coefficient of the saturated matrix corresponds to $\lambda_f = \lambda + \beta^2 m$. A summary of all the model coefficients together with their physical meaning and unit of measure is given in Table 3 below. To be consistent, in (2.2) we consider the same viscous model as in (2.1). We remark that other viscous models can be considered in both equations, see e.g. [60], but are beyond the scope of this work.

Poroelastic-elastic coupling. On Γ_I the coupling between the elastic and the poroelastic domains is achieved by imposing the following transmission conditions, expressing continuity of the normal stresses, the continuity of displacements, and the absence of fluid flow into the elastic domain:

$$(2.4) \qquad \boldsymbol{\sigma}_e(\boldsymbol{u}_e)\boldsymbol{n}_p = \boldsymbol{\sigma}_e(\boldsymbol{u}_p)\boldsymbol{n}_p - \delta\beta\, p(\boldsymbol{u}_p, \boldsymbol{u}_f)\boldsymbol{I}\boldsymbol{n}_p, \qquad \text{in } \Gamma_I \times (0, T],$$

$$(2.5) \qquad\qquad\qquad \boldsymbol{u}_e = \boldsymbol{u}_p, \qquad\qquad\qquad\qquad \text{in } \Gamma_I \times (0, T],$$

$$(2.6) \qquad ((1 - \delta)\beta\boldsymbol{u}_p + \boldsymbol{u}_f) \cdot \boldsymbol{n}_p = 0, \qquad\qquad \text{in } \Gamma_I \times (0, T],$$

for $\delta \in [0, 1]$ representing the fluid entry resistance of the interface. In the case $\delta = 1$, condition (2.6) reduces to $\boldsymbol{u}_f \cdot \boldsymbol{n}_p = 0$, namely there is no filtration through the interface; whereas if $1 - \delta = \phi\beta^{-1} < 1$, then (2.6) imposes that the normal component of the fluid displacement $\boldsymbol{u}_p + \phi^{-1}\boldsymbol{u}_f$ is zero, meaning that the fluid is partially flowing into the interface. This assumption on the coupling conditions is somewhat similar to the one that is considered [9] for the poroelastic–acoustic case. For the latter, the continuity of the pressure at the interface was a function of the parameter $\tau \in [0, 1]$ modeling the closing/opening of the pores at the interface.

Coupled problem. Supplementing the previous constitutive equations with homogeneous Dirichlet boundary conditions, the coupled *poroelastic-elastic problem* reads: for any $t \in (0, T]$, find the vector-fields $\mathsf{U} = (\boldsymbol{u}_e, \boldsymbol{u}_p, \boldsymbol{u}_f) : \Omega_e \times \Omega_p \times \Omega_p \to \mathbb{R}$ such that (2.1)–(2.2) coupled with (2.4)–(2.6) hold. Finally, we close the problem by considering initial conditions $\mathsf{U}(\cdot, 0) = \mathsf{U}_0 = (\boldsymbol{u}_{0e}, \boldsymbol{u}_{0p}, \boldsymbol{u}_{0f})$ and $\dot{\mathsf{U}}(\cdot, 0) = \mathsf{V}_0 = (\boldsymbol{v}_{0e}, \boldsymbol{v}_{0p}, \boldsymbol{v}_{0f})$.

2.1. Weak formulation and stability estimates. In order to state the weak formulation taking into account the essential boundary conditions, we also introduce the subspaces

$$\boldsymbol{V}^i = \{\boldsymbol{v} \in \boldsymbol{H}^1(\Omega_i) \,|\, \boldsymbol{v}_{|\Gamma_i} = \boldsymbol{0}\}, \ i = \{e, p\},$$

$$\boldsymbol{W}^p = \{\boldsymbol{z} \in \boldsymbol{H}(\mathrm{div}, \Omega_p) \,|\, (\boldsymbol{z} \cdot \boldsymbol{n}_p)_{|\Gamma_p} = 0\}.$$

and define the Hilbert spaces $\boldsymbol{V}_0 = \boldsymbol{L}^2(\Omega_e) \times \boldsymbol{L}^2(\Omega_p) \times \boldsymbol{L}^2(\Omega_p)$ and $\boldsymbol{V} = \boldsymbol{V}^e \times \boldsymbol{V}^p \times \boldsymbol{W}^p$, endowed with the following norm and seminorm, respectively

$$\|\mathsf{U}\|_0^2 = \|\rho_e^{1/2}\boldsymbol{u}_e\|_{\Omega_e}^2 + \|\rho_u^{1/2}\boldsymbol{u}_p\|_{\Omega_p}^2 + \|(\rho_f\phi)^{1/2}(\boldsymbol{u}_p + \phi^{-1}\boldsymbol{u}_f)\|_{\Omega_p}^2 \quad \forall \mathsf{U} \in \boldsymbol{V}_0,$$

$$|\mathsf{U}|_{\boldsymbol{V}}^2 = \|\mathbb{C}^{1/2} : \boldsymbol{\epsilon}(\boldsymbol{u}_e)\|_{\Omega_e}^2 + \|\rho_e^{1/2}\zeta\boldsymbol{u}_e\|_{\Omega_e}^2 + \|\mathbb{C}^{1/2} : \boldsymbol{\epsilon}(\boldsymbol{u}_p)\|_{\Omega_p}^2 + \|\rho^{1/2}\zeta\boldsymbol{u}_p\|_{\Omega_p}^2$$

$$+ \|m^{1/2}\nabla \cdot (\beta\boldsymbol{u}_p + \boldsymbol{u}_f)\|_{\Omega_p}^2 \quad \forall \mathsf{U} \in \boldsymbol{V},$$

where $\rho_u = (1 - \phi)\rho_s/2$. The weak form of (2.1)–(2.6) reads as: for any $t \in (0, T]$, find $\mathsf{U} \in \boldsymbol{V}$ s.t. $\boldsymbol{u}_e = \boldsymbol{u}_p$ on Γ_I and

$$(2.7) \qquad \mathcal{M}(\ddot{\mathsf{U}}, \mathsf{V}) + \mathcal{D}(\dot{\mathsf{U}}, \mathsf{V}) + \mathcal{A}(\mathsf{U}, \mathsf{V}) + \mathcal{C}(\mathsf{U}, \mathsf{V}) = \mathcal{F}(\mathsf{V}) \quad \forall\, \mathsf{V} \in \boldsymbol{V},$$

with $\mathsf{U}(\cdot,0) = \mathsf{U}_0 \in \boldsymbol{V}$ and $\dot{\mathsf{U}}(\cdot,0) = \mathsf{V}_0 \in \boldsymbol{V}_0$. In (2.7) $\mathcal{F} : \Omega_e \times \Omega_p \times \Omega_p \to \mathbb{R}$ is a linear functional defined as

$$\mathcal{F}(\mathsf{V}) = (\boldsymbol{f}_e, \boldsymbol{v}_e)_{\Omega_e} + (\boldsymbol{f}_p, \boldsymbol{v}_p)_{\Omega_p} + (\boldsymbol{g}_p, \boldsymbol{v}_f)_{\Omega_p}$$

for any $\mathsf{V} = (\boldsymbol{v}_e, \boldsymbol{v}_p, \boldsymbol{v}_f) \in \boldsymbol{V}$, while for any $\mathsf{U}, \mathsf{V} \in \boldsymbol{V}$ we have set
(2.8)
$$\mathcal{M}(\mathsf{U},\mathsf{V}) = (\rho_e \boldsymbol{u}_e, \boldsymbol{v}_e)_{\Omega_e} + (\rho_p \boldsymbol{u}_p + \rho_f \boldsymbol{u}_f, \boldsymbol{v}_p)_{\Omega_p} + (\rho_f \boldsymbol{u}_p + \rho_w \boldsymbol{u}_f, \boldsymbol{v}_f)_{\Omega_p},$$

$$\mathcal{D}(\mathsf{U},\mathsf{V}) = (2\rho_e \zeta \boldsymbol{u}_e, \boldsymbol{v}_e)_{\Omega_e} + (2\rho_p \zeta \boldsymbol{u}_p, \boldsymbol{v}_p)_{\Omega_p} + (\eta k^{-1} \boldsymbol{u}_f, \boldsymbol{v}_f)_{\Omega_p},$$

$$\mathcal{A}(\mathsf{U},\mathsf{V}) = (\boldsymbol{\sigma}_e(\boldsymbol{u}_e), \boldsymbol{\epsilon}(\boldsymbol{v}_e))_{\Omega_e} + (\rho_e \zeta^2 \boldsymbol{u}_e, \boldsymbol{v}_e)_{\Omega_e} + (\boldsymbol{\sigma}_e(\boldsymbol{u}_p), \boldsymbol{\epsilon}(\boldsymbol{v}_p))_{\Omega_p} + (\rho_p \zeta^2 \boldsymbol{u}_p, \boldsymbol{v}_p)_{\Omega_p}$$
$$+ (m \nabla \cdot (\beta \boldsymbol{u}_p + \boldsymbol{u}_f), \nabla \cdot (\beta \boldsymbol{v}_p + \boldsymbol{v}_f))_{\Omega_p}$$

$$\mathcal{C}(\mathsf{U},\mathsf{V}) = -\langle \boldsymbol{\sigma}_e(\boldsymbol{u}_e) \boldsymbol{n}_p, \boldsymbol{v}_p - \boldsymbol{v}_e \rangle_{\Gamma_I} + \langle p(\boldsymbol{u}_p, \boldsymbol{u}_f), ((1-\delta)\beta \boldsymbol{v}_p + \boldsymbol{v}_f) \cdot \boldsymbol{n}_p \rangle_{\Gamma_I},$$

with $\langle \cdot, \cdot \rangle_{\Gamma_I}$ in (2.8) denoting the $H^{\frac{1}{2}}(\Gamma_I)$-$H^{-\frac{1}{2}}(\Gamma_I)$ duality product. Before presenting a stability estimate for the solution of problem (2.7) we define, for all $\mathsf{U} \in C^1([0,T];\boldsymbol{V}_0) \cap C^0([0,T];\boldsymbol{V})$, the energy norm

$$(2.9) \quad \|\mathsf{U}(t)\|_{\mathcal{E}}^2 = \|\dot{\mathsf{U}}(t)\|_0^2 + |\mathsf{U}(t)|_{\boldsymbol{V}}^2 + \int_0^t \mathcal{D}(\dot{\mathsf{U}}, \dot{\mathsf{U}})(s)\, ds + \mathcal{D}(\mathsf{U},\mathsf{U})(0) \quad t \in (0,T],$$

and we adopt the notation $\|\mathsf{U}_0\|_{\mathcal{E}}^2 = \|\mathsf{U}(0)\|_{\mathcal{E}}^2 = \|\mathsf{V}_0\|_0^2 + |\mathsf{U}_0|_{\boldsymbol{V}}^2 + \mathcal{D}(\mathsf{U}_0, \mathsf{U}_0)$. As a result of Lemma 2.1 below, $\max_{0 \le t \le T} \| \cdot \|_{\mathcal{E}}$ is a norm on $C^1([0,T];\boldsymbol{V}_0) \cap C^0([0,T];\boldsymbol{V})$.

LEMMA 2.1. *The bilinear forms $\mathcal{M}$, $\mathcal{D}$, and $\mathcal{A}$ defined in (2.8) are such that*

$$(2.10) \qquad\qquad \mathcal{M}(\mathsf{U},\mathsf{V}) \lesssim \|\mathsf{U}\|_0 \|\mathsf{V}\|_0 \qquad\qquad \forall \mathsf{U}, \mathsf{V} \in \boldsymbol{V}_0,$$

$$(2.11) \qquad\qquad \mathcal{M}(\mathsf{U},\mathsf{U}) \gtrsim \|\mathsf{U}\|_0^2 \qquad\qquad\qquad \forall \mathsf{U} \in \boldsymbol{V}_0,$$

$$(2.12) \qquad\qquad \mathcal{A}(\mathsf{U},\mathsf{V}) \lesssim |\mathsf{U}|_{\boldsymbol{V}} |\mathsf{V}|_{\boldsymbol{V}} \qquad\qquad \forall \mathsf{U}, \mathsf{V} \in \boldsymbol{V},$$

$$(2.13) \qquad\qquad \mathcal{A}(\mathsf{U},\mathsf{U}) = |\mathsf{U}|_{\boldsymbol{V}}^2 \qquad\qquad\qquad \forall \mathsf{U} \in \boldsymbol{V}.$$

Proof. Inequalities (2.10) and (2.12) are readily inferred by applying the Cauchy–Schwarz and triangle inequalities. For (2.11) we use the definition of the density functions ρ_e, ρ_p, ρ_u, and ρ_w, we observe that $a > 1$ to prove that $\mathcal{M}(\mathsf{U},\mathsf{U}) \gtrsim \|\mathsf{U}\|_0^2$, cf. [8]. The last equality (2.13) follows by the definition (2.8). $\qquad\square$

THEOREM 2.2 (Stability of the continuous weak formulation). *Assume that the problem data satisfy $\mathsf{F} = (\boldsymbol{f}_e, \boldsymbol{f}_p, \boldsymbol{g}_p) \in L^2((0,T);\boldsymbol{V}_0)$, $\mathsf{U}_0 \in \boldsymbol{V}$, and $\mathsf{V}_0 \in \boldsymbol{V}_0$. For any $t \in (0,T]$, let $\mathsf{U} = (\boldsymbol{u}_e, \boldsymbol{u}_p, \boldsymbol{u}_f) \in \boldsymbol{V}$ be the solution of (2.7). Then, it holds*

$$\max_{0 \le t \le T} \|\mathsf{U}(t)\|_{\mathcal{E}}^2 \lesssim \|\mathsf{U}_0\|_{\mathcal{E}}^2 + \int_0^T \left(\|(2\rho_e \zeta)^{-1/2} \boldsymbol{f}_e\|_{\Omega_e}^2 + \|(2\rho_e \zeta)^{-1/2} \boldsymbol{f}_p\|_{\Omega_p}^2 \right.$$
$$\left. + \|(\eta/k)^{-1/2} \boldsymbol{g}_p\|_{\Omega_p}^2 \right) ds,$$

with hidden constant depending on the observation time t and the material properties.

Proof. The proof follows the lines of the one proposed in [8, Proposition 5.1]. We take $\dot{\mathsf{U}} = (\dot{\boldsymbol{u}}_e, \dot{\boldsymbol{u}}_p, \dot{\boldsymbol{u}}_f)$ as test functions in (2.7) so that the interface terms are null, i.e., $\mathcal{C}(\mathsf{U}, \dot{\mathsf{U}}) = 0$, thanks to condition (2.5). We integrate in time between 0 and t, add on both side $\mathcal{D}(\mathsf{U}_0, \mathsf{U}_0) \ge 0$, and use (2.10)–(2.13) to get

$$\|\mathsf{U}(t)\|_{\mathcal{E}}^2 + \int_0^t \mathcal{D}(\dot{\mathsf{U}}, \dot{\mathsf{U}})(s)\, ds \lesssim \|\mathsf{U}_0\|_{\mathcal{E}}^2 + 2 \int_0^t \mathcal{F}(\dot{\mathsf{U}})(s)\, ds.$$

The thesis follows by applying the Cauchy-Schwarz and Young inequalities to bound the second term on the right-hand side.   □

3. Semi-discrete formulation and stability analysis. We introduce a *polytopic* mesh $\mathcal{T}_h$ made of general polygons (in 2d) or polyhedra (in 3d) and write $\mathcal{T}_h$ as $\mathcal{T}_h = \mathcal{T}_h^e \cup \mathcal{T}_h^p$, where $\mathcal{T}_h^\# = \{\kappa \in \mathcal{T}_h : \overline{\kappa} \subseteq \overline{\Omega}_\#\}$, with $\# = \{e, p\}$. Implicit in this decomposition there is the assumption that the meshes $\mathcal{T}_h^e$ and $\mathcal{T}_h^p$ are aligned with Ω_e and Ω_p, respectively. Polynomial degrees $p_{e,\kappa} \geq 1$ and $p_{p,\kappa} \geq 1$ are associated with each element of $\mathcal{T}_h^e$ and $\mathcal{T}_h^p$. The discrete spaces are introduced as follows: $\boldsymbol{V}_h^e = [\mathcal{P}_{p_e}(\mathcal{T}_h^e)]^d$ and $\boldsymbol{V}_h^p = [\mathcal{P}_{p_p}(\mathcal{T}_h^p)]^d$ where $\mathcal{P}_r(\mathcal{T}_h^\#)$ is the space of piecewise polynomials in $\Omega_\#$ of total degree less than or equal to r_κ in any $\kappa \in \mathcal{T}_h^\#$ with $\# = \{e, p\}$.

In the following, we assume that $\mathbb{C}$ and m are element-wise constant and we define $\overline{\mathbb{C}}_\kappa = (|\mathbb{C}^{1/2}|_2^2)_{|\kappa}$ for all $\kappa \in \mathcal{T}_h^e \cup \mathcal{T}_h^p$, and $\overline{m}_\kappa = (m)_{|\kappa}$ for all $\kappa \in \mathcal{T}_h^p$. The symbol $|\cdot|_2$ stands for the ℓ^2-norm on $\mathbb{R}^{n \times n}$, with $n = 3$ if $d = 2$ and $n = 6$ if $d = 3$. In order to deal with polygonal and polyhedral elements, we define an *interface* as the intersection of the $(d-1)$-dimensional faces of any two neighboring elements of $\mathcal{T}_h$. If $d = 2$, an interface/face is a line segment and the set of all interfaces/faces is denoted by $\mathcal{F}_h$. When $d = 3$, an interface can be a general polygon that we assume could be further decomposed into a set of planar triangles collected in the set $\mathcal{F}_h$. We decompose $\mathcal{F}_h$ as $\mathcal{F}_h = \mathcal{F}_h^I \cup \mathcal{F}_h^e \cup \mathcal{F}_h^p$, where $\mathcal{F}_h^I = \{F \in \mathcal{F}_h : F \subset \partial\kappa^e \cap \partial\kappa^p, \kappa^e \in \mathcal{T}_h^e, \kappa^p \in \mathcal{T}_h^p\}$, and $\mathcal{F}_h^e$, and $\mathcal{F}_h^p$ denote all the faces of $\mathcal{T}_h^e$, and $\mathcal{T}_h^p$ respectively, not laying on Γ_I. Finally, the faces of $\mathcal{T}_h^e$ and $\mathcal{T}_h^p$ can be further written as the union of *internal* (i) and *boundary* (b) faces, respectively, i.e.: $\mathcal{F}_h^e = \mathcal{F}_h^{e,i} \cup \mathcal{F}_h^{e,0}$ and $\mathcal{F}_h^p = \mathcal{F}_h^{p,i} \cup \mathcal{F}_h^{p,0}$.

Following [29], we next introduce the main assumption on $\mathcal{T}_h$.

DEFINITION 3.1. *A mesh $\mathcal{T}_h$ is said to be polytopic-regular if for any $\kappa \in \mathcal{T}_h$, there exists a set of non-overlapping d-dimensional simplices contained in κ, denoted by $\{S_\kappa^F\}_{F \subset \partial\kappa}$, such that for any face $F \subset \partial\kappa$, it holds $h_\kappa \lesssim d|S_\kappa^F| |F|^{-1}$.*

ASSUMPTION 3.1. *The sequence of meshes $\{\mathcal{T}_h\}_h$ is assumed to be uniformly polytopic regular in the sense of Definition 3.1.*

As pointed out in [29], this assumption does not impose any restriction on either the number of faces per element nor their measure relative to the diameter of the element they belong to. Under Assumption 3.1, the following *trace-inverse inequality* holds:

$$(3.1) \qquad ||v||_{L^2(\partial\kappa)} \lesssim p h_\kappa^{-1/2} ||v||_{L^2(\kappa)} \qquad\qquad \forall \, \kappa \in \mathcal{T}_h \; \forall v \in \mathcal{P}_p(\kappa).$$

In order to avoid technicalities, we also assume that $\mathcal{T}_h$ satisfies a *hp-local bounded variation* property:

ASSUMPTION 3.2. *For any pair of neighboring elements $\kappa^\pm \in \mathcal{T}_h^\#$, it holds $h_{\kappa^+} \lesssim h_{\kappa^-} \lesssim h_{\kappa^+}$, $p_{\#,\kappa^+} \lesssim p_{\#,\kappa^-} \lesssim p_{\#,\kappa^+}$, with $\# = \{e, p\}$.*

Finally, following [16], for sufficiently piecewise smooth scalar-, vector- and tensor-valued fields ψ, $\boldsymbol{v}$ and $\boldsymbol{\tau}$, respectively, we define the averages and jumps on each *interior* face $F \in \mathcal{F}_h^{e,i} \cup \mathcal{F}_h^{p,i} \cup \mathcal{F}_h^I$ shared by the elements $\kappa^\pm \in \mathcal{T}_h$ as follows:

$$[\![\psi]\!] = \psi^+ \boldsymbol{n}^+ + \psi^- \boldsymbol{n}^-, \quad [\![\boldsymbol{v}]\!] = \boldsymbol{v}^+ \otimes \boldsymbol{n}^+ + \boldsymbol{v}^- \otimes \boldsymbol{n}^-, \quad [\![\boldsymbol{v}]\!]_n = \boldsymbol{v}^+ \cdot \boldsymbol{n}^+ + \boldsymbol{v}^- \cdot \boldsymbol{n}^-,$$

$$\{\!\{\psi\}\!\} = \frac{\psi^+ + \psi^-}{2}, \qquad \{\!\{\boldsymbol{v}\}\!\} = \frac{\boldsymbol{v}^+ + \boldsymbol{v}^-}{2}, \qquad\qquad \{\!\{\boldsymbol{\tau}\}\!\} = \frac{\boldsymbol{\tau}^+ + \boldsymbol{\tau}^-}{2},$$

where $\otimes$ is the tensor product in $\mathbb{R}^3$, $\cdot^\pm$ denotes the trace on F taken within $\kappa^\pm$, and $\boldsymbol{n}^\pm$ is the outer normal vector to $\partial\kappa^\pm$. Accordingly, on *boundary* faces $F \in \mathcal{F}_h^{e,0} \cup \mathcal{F}_h^{p,0}$, we set $[\![\psi]\!] = \psi\boldsymbol{n}$, $\{\!\{\psi\}\!\} = \psi$, $[\![\boldsymbol{v}]\!] = \boldsymbol{v} \otimes \boldsymbol{n}$, $[\![\boldsymbol{v}]\!]_n = \boldsymbol{v} \cdot \boldsymbol{n}$, $\{\!\{\boldsymbol{v}\}\!\} = \boldsymbol{v}$, $\{\!\{\boldsymbol{\tau}\}\!\} = \boldsymbol{\tau}$.

For later use, we also define ∇_h and $\nabla_h\cdot$ to be the broken gradient and divergence operators, respectively, set $\boldsymbol{\epsilon}_h(\boldsymbol{v}) = \frac{\nabla_h\boldsymbol{v}+\nabla_h\boldsymbol{v}^T}{2}$, $\boldsymbol{\sigma}_{eh}(\boldsymbol{v}) = \mathbb{C} : \boldsymbol{\epsilon}_h(\boldsymbol{v})$, and use the shorthand notation $(\cdot,\cdot)_{\Omega_\#} = \sum_{\kappa\in\mathcal{T}_h^\#}\int_\kappa\cdot$ and $\langle\cdot,\cdot\rangle_{\mathcal{F}_h^\#} = \sum_{F\in\mathcal{F}_h^\#}\int_F\cdot$ for $\# = \{e,p\}$.

3.1. Semi-discrete PolydG formulation. We define the space $\boldsymbol{V}_h = \boldsymbol{V}_h^e \times \boldsymbol{V}_h^p \times \boldsymbol{V}_h^p$ and denote by $\mathsf{U}_h = (\boldsymbol{u}_e, \boldsymbol{u}_p, \boldsymbol{u}_f)_h$ a generic function in $\boldsymbol{V}_h$. The semi-discrete PolydG formulation of problem (2.7) reads as: find $\mathsf{U}_h \in \boldsymbol{V}_h$ such that

$$(3.2) \quad \mathcal{M}(\ddot{\mathsf{U}}_h, \mathsf{V}_h) + \mathcal{D}(\dot{\mathsf{U}}_h, \mathsf{V}_h) + \mathcal{A}_h(\mathsf{U}_h, \mathsf{V}_h) + \mathcal{C}_h(\mathsf{U}_h, \mathsf{V}_h) = \mathcal{F}(\mathsf{V}_h) \quad \forall \mathsf{V}_h \in \boldsymbol{V}_h.$$

As initial conditions we take suitable projections onto $\boldsymbol{V}_h$ of the initial data, namely $\mathsf{U}_h(0) = \mathsf{U}_{0h}$ and $\dot{\mathsf{U}}_h(0) = \mathsf{V}_{0h}$. The bilinear forms $\mathcal{M}$ and $\mathcal{D}$ appearing in (3.2) are defined as in (2.8) while

$$(3.3) \quad \mathcal{A}_h(\mathsf{U}, \mathsf{V}) = \mathcal{A}_h^e(\boldsymbol{u}_e, \boldsymbol{v}_e) + \mathcal{A}_h^p(\boldsymbol{u}_p, \boldsymbol{v}_p) + \mathcal{B}_h^p(\beta\boldsymbol{u}_p + \boldsymbol{u}_f, \beta\boldsymbol{v}_p + \boldsymbol{v}_f)$$

for all $\mathsf{U} = (\boldsymbol{u}_e, \boldsymbol{u}_p, \boldsymbol{u}_f)$ and $\mathsf{V} = (\boldsymbol{v}_e, \boldsymbol{v}_p, \boldsymbol{v}_f) \in \boldsymbol{V}_h$ with

$$
\begin{aligned}
(3.4) \quad \mathcal{A}_h^\star(\boldsymbol{u}_\star, \boldsymbol{v}_\star) &= (\boldsymbol{\sigma}_{eh}(\boldsymbol{u}_\star), \boldsymbol{\epsilon}_h(\boldsymbol{v}_\star))_{\Omega_\star} + (\rho_\star\zeta^2\boldsymbol{u}_\star, \boldsymbol{v}_\star)_{\Omega_\star} - \langle\{\boldsymbol{\sigma}_{eh}(\boldsymbol{u}_\star)\}, [\![\boldsymbol{v}_\star]\!]\rangle_{\mathcal{F}_h^\star} \\
&\quad - \langle[\![\boldsymbol{u}_\star]\!], \{\boldsymbol{\sigma}_{eh}(\boldsymbol{v}_\star)\}\rangle_{\mathcal{F}_h^\star} + \langle\alpha[\![\boldsymbol{u}_\star]\!], [\![\boldsymbol{v}_\star]\!]\rangle_{\mathcal{F}_h^\star}, \quad \star = \{e, p\}, \\
\mathcal{B}_h^p(\boldsymbol{u}, \boldsymbol{v}) &= (m\nabla_h\cdot\boldsymbol{u}, \nabla_h\cdot\boldsymbol{v})_\Omega - \langle\{m(\nabla_h\cdot\boldsymbol{u})\}, [\![\boldsymbol{v}]\!]_{\boldsymbol{n}}\rangle_{\mathcal{F}_h^p} \\
&\quad - \langle[\![\boldsymbol{u}]\!]_{\boldsymbol{n}}, \{m(\nabla_h\cdot\boldsymbol{v})\}\rangle_{\mathcal{F}_h^p} + \langle\gamma[\![\boldsymbol{u}]\!]_{\boldsymbol{n}}, [\![\boldsymbol{v}]\!]_{\boldsymbol{n}}\rangle_{\mathcal{F}_h^p},
\end{aligned}
$$

cf also [9]. Here, the stabilization functions $\alpha \in L^\infty(\mathcal{F}_h^\star)$, for $\star = \{p, e\}$ and $\gamma \in L^\infty(\mathcal{F}_h^p)$ are defined s.t.

$$(3.5) \quad \alpha|_F = \begin{cases} c_1 \max\limits_{\kappa\in\{\kappa^+,\kappa^-\}} \left(\overline{\mathbb{C}}_\kappa\, p_{\star,\kappa}^2 h_\kappa^{-1}\right) & \forall F \in \mathcal{F}_h^{\star,i} \cup \mathcal{F}_h^I, F \subseteq \partial\kappa^+ \cap \partial\kappa^-, \\ \overline{\mathbb{C}}_\kappa\, p_{\star,\kappa}^2 h_\kappa^{-1} & \forall F \in \mathcal{F}_h^{\star,b}, \qquad F \subseteq \partial\kappa, \end{cases}$$

$$(3.6) \quad \gamma|_F = \begin{cases} c_2 \max\limits_{\kappa\in\{\kappa^+,\kappa^-\}} \left(\overline{m}_\kappa\, p_{p,\kappa}^2 h_\kappa^{-1}\right) & \forall F \in \mathcal{F}_h^{p,i}, \qquad F \subseteq \partial\kappa^+ \cap \partial\kappa^-, \\ \overline{m}_\kappa\, p_{p,\kappa}^2 h_\kappa^{-1} & \forall F \in \mathcal{F}_h^{p,b} \cup \mathcal{F}_h^I, F \subseteq \partial\kappa, \kappa \in \mathcal{T}_h^p, \end{cases}$$

with positive constants c_1 and c_2 that have to be properly chosen. The definition of the penalty functions (3.5)–(3.6) is based on [29, Lemma 35]. Alternative stabilization functions can be defined in the spirit of [2]. The analysis of the latter is however beyond the scope of this work. The bilinear form $\mathcal{C}_h(\cdot,\cdot)$ is responsible for the coupling between the elastic and the poroelastic domain and is defined as the sum of five contributions, namely

$$
\begin{aligned}
\mathcal{C}_h(\mathsf{U}, \mathsf{V}) &= \mathcal{A}_{\Gamma_I}^e(\boldsymbol{u}_e, \boldsymbol{v}_e) + \mathcal{A}_{\Gamma_I}^p(\boldsymbol{u}_p, \boldsymbol{v}_p) + \mathcal{B}_{\Gamma_I}^{pp}(\boldsymbol{u}_p, \boldsymbol{v}_p) + \mathcal{B}_{\Gamma_I}^{pf}(\boldsymbol{u}_p, \boldsymbol{v}_f) \\
&\quad + \mathcal{B}_{\Gamma_I}^{fp}(\boldsymbol{u}_f, \boldsymbol{v}_p) + \mathcal{B}_{\Gamma_I}^{ff}(\boldsymbol{u}_f, \boldsymbol{v}_f) + \mathcal{C}_{\Gamma_I}^{ep}(\boldsymbol{u}_e, \boldsymbol{v}_p) + \mathcal{C}_{\Gamma_I}^{pe}(\boldsymbol{u}_p, \boldsymbol{v}_e),
\end{aligned}
$$

for any $\mathsf{U}, \mathsf{V} \in \boldsymbol{V}_h$, where

$$
\begin{aligned}
&(3.7) \\
&\mathcal{A}_{\Gamma_I}^e(\boldsymbol{u}_e, \boldsymbol{v}_e) = \langle\boldsymbol{\sigma}_{eh}(\boldsymbol{u}_e)\boldsymbol{n}_p, \boldsymbol{v}_e\rangle_{\mathcal{F}_h^I} + \langle\boldsymbol{\sigma}_{eh}(\boldsymbol{v}_e)\boldsymbol{n}_p, \boldsymbol{u}_e\rangle_{\mathcal{F}_h^I} + \langle\alpha\boldsymbol{u}_e, \boldsymbol{v}_e\rangle_{\mathcal{F}_h^I}, \\
&\mathcal{A}_{\Gamma_I}^p(\boldsymbol{u}_p, \boldsymbol{v}_p) = \langle\alpha\boldsymbol{u}_p, \boldsymbol{v}_p\rangle_{\mathcal{F}_h^I},
\end{aligned}
$$

$$\mathcal{B}_{\Gamma_I}^{pp}(\boldsymbol{u}_p, \boldsymbol{v}_p) = - \langle m\beta\nabla_h \cdot \boldsymbol{u}_p, (1-\delta)\beta\boldsymbol{v}_p \cdot \boldsymbol{n}_p\rangle_{\mathcal{F}_h^I} - \langle m\beta\nabla_h \cdot \boldsymbol{v}_p, (1-\delta)\beta\boldsymbol{u}_p \cdot \boldsymbol{n}_p\rangle_{\mathcal{F}_h^I}$$
$$+ \langle \gamma(1-\delta)\beta\boldsymbol{u}_p \cdot \boldsymbol{n}_p, (1-\delta)\beta\boldsymbol{v}_p \cdot \boldsymbol{n}_p\rangle_{\mathcal{F}_h^I},$$

$$\mathcal{B}_{\Gamma_I}^{pf}(\boldsymbol{u}_p, \boldsymbol{v}_f) = - \langle m\beta\nabla_h \cdot \boldsymbol{u}_p, \boldsymbol{v}_f \cdot \boldsymbol{n}_p\rangle_{\mathcal{F}_h^I} - \langle m\nabla_h \cdot \boldsymbol{v}_f, (1-\delta)\beta\boldsymbol{u}_p \cdot \boldsymbol{n}_p\rangle_{\mathcal{F}_h^I}$$
$$+ \langle \gamma(1-\delta)\beta\boldsymbol{u}_p \cdot \boldsymbol{n}_p, \boldsymbol{v}_f \cdot \boldsymbol{n}_p\rangle_{\mathcal{F}_h^I},$$

$$\mathcal{B}_{\Gamma_I}^{fp}(\boldsymbol{u}_f, \boldsymbol{v}_p) = - \langle m\nabla_h \cdot \boldsymbol{u}_f, (1-\delta)\beta\boldsymbol{v}_p \cdot \boldsymbol{n}_p\rangle_{\mathcal{F}_h^I} - \langle m\beta\nabla_h \cdot \boldsymbol{v}_p, \boldsymbol{u}_f \cdot \boldsymbol{n}_p\rangle_{\mathcal{F}_h^I}$$
$$+ \langle \gamma\boldsymbol{u}_f \cdot \boldsymbol{n}_p, (1-\delta)\beta\boldsymbol{v}_p \cdot \boldsymbol{n}_p\rangle_{\mathcal{F}_h^I},$$

$$\mathcal{B}_{\Gamma_I}^{ff}(\boldsymbol{u}_f, \boldsymbol{v}_f) = - \langle m\nabla_h \cdot \boldsymbol{u}_f, \boldsymbol{v}_f \cdot \boldsymbol{n}_p\rangle_{\mathcal{F}_h^I} - \langle m\nabla_h \cdot \boldsymbol{v}_f, \boldsymbol{u}_f \cdot \boldsymbol{n}_p\rangle_{\mathcal{F}_h^I}$$
$$+ \langle \gamma\boldsymbol{u}_f \cdot \boldsymbol{n}_p, \boldsymbol{v}_f \cdot \boldsymbol{n}_p\rangle_{\mathcal{F}_h^I},$$

$$\mathcal{C}_{\Gamma_I}^{ep}(\boldsymbol{u}_e, \boldsymbol{v}_p) = - \langle \boldsymbol{\sigma}_{eh}(\boldsymbol{u}_e)\boldsymbol{n}_p, \boldsymbol{v}_p\rangle_{\mathcal{F}_h^I} - \langle \alpha\boldsymbol{u}_e, \boldsymbol{v}_p\rangle_{\mathcal{F}_h^I},$$

$$\mathcal{C}_{\Gamma_I}^{pe}(\boldsymbol{u}_p, \boldsymbol{v}_e) = - \langle \boldsymbol{\sigma}_{eh}(\boldsymbol{v}_e)\boldsymbol{n}_p, \boldsymbol{u}_p\rangle_{\mathcal{F}_h^I} - \langle \alpha\boldsymbol{u}_p, \boldsymbol{v}_e\rangle_{\mathcal{F}_h^I}.$$

The derivation of the coupling bilinear form $\mathcal{C}_h(\cdot, \cdot)$, starting from the strong formulation of the poroelastic-elastic problem, is detailed in the Appendix.

Remark 3.2. Notice that the coupling conditions (2.4) and (2.5) are imposed (weakly) through the bilinear forms $\mathcal{A}_{\Gamma_I}^e(\cdot, \cdot), \mathcal{A}_{\Gamma_I}^p(\cdot, \cdot), \mathcal{C}_{\Gamma_I}^{ep}(\cdot, \cdot)$ and $\mathcal{C}_{\Gamma_I}^{pe}(\cdot, \cdot)$, while condition (2.6) is included in the bilinear forms $\mathcal{B}_{\Gamma_I}^{pp}(\cdot, \cdot), \mathcal{B}_{\Gamma_I}^{pf}(\cdot, \cdot), \mathcal{B}_{\Gamma_I}^{fp}(\cdot, \cdot)$, and $\mathcal{B}_{\Gamma_I}^{ff}(\cdot, \cdot)$. The latter couples at the interface the filtration displacement in Ω_p to the elastic displacement in Ω_e, through the elastic displacement in Ω_p.

By fixing a basis for the space $\boldsymbol{V}_h$ and denoting by $\mathsf{U}_h = (\mathbf{U}_e, \mathbf{U}_p, \mathbf{U}_f)^T \in \mathbb{R}^{\mathsf{ndof}}$ the vector of the ndof expansion coefficients in the chosen basis of the unknown U_h, the semi-discrete formulation (3.2) can be written equivalently as:

$$(3.8) \quad \begin{bmatrix} M_{\rho_e}^e & 0 & 0 \\ 0 & M_\rho^p & M_{\rho_f}^p \\ 0 & M_{\rho_f}^p & M_{\rho_w}^p \end{bmatrix} \begin{bmatrix} \ddot{\mathbf{U}}_e \\ \ddot{\mathbf{U}}_p \\ \ddot{\mathbf{U}}_f \end{bmatrix} + \begin{bmatrix} D_{\rho_e}^e & 0 & 0 \\ 0 & D_\rho^p & 0 \\ 0 & 0 & D^f \end{bmatrix} \begin{bmatrix} \dot{\mathbf{U}}_e \\ \dot{\mathbf{U}}_p \\ \dot{\mathbf{U}}_f \end{bmatrix}$$
$$+ \begin{bmatrix} A_h^e + A_{\Gamma_I}^e & C_{\Gamma_I}^{pe} & 0 \\ C_{\Gamma_I}^{ep} & A^p + A_{\Gamma_I}^p + B_{\beta^2}^p + B_{\Gamma_I}^{pp} & B_\beta^p + B_{\Gamma_I}^{fp} \\ 0 & B_\beta^p + B_{\Gamma_I}^{pf} & B^p + B_{\Gamma_I}^{ff} \end{bmatrix} \begin{bmatrix} \mathbf{U}_e \\ \mathbf{U}_p \\ \mathbf{U}_f \end{bmatrix} = \begin{bmatrix} \mathbf{F}^e \\ \mathbf{F}^p \\ \mathbf{G}^p \end{bmatrix}$$

with initial conditions $\mathbf{U}_{0h}$ and $\mathbf{V}_{0h}$. We remark that $\mathbf{F}^e, \mathbf{F}^p$ and $\mathbf{G}^p$ are the vector representations of the linear functional $\mathcal{F}$. To ease the notation, we set $\mathbf{F}_h = [\mathbf{F}^e, \mathbf{F}^p, \mathbf{G}^p]^T$ and we rewrite system (3.8) in compact form as

$$(3.9) \qquad M\ddot{\mathbf{U}}_h(t) + D\dot{\mathbf{U}}_h(t) + (A + B + C)\mathbf{U}_h(t) = \mathbf{F}_h(t) \quad \forall t \in (0, T].$$

3.2. Stability analysis. To carry out the stability analysis of the semi-discrete problem, we introduce the energy norm

$$(3.10) \quad \|\mathsf{U}(t)\|_{\mathrm{E}}^2 = \|\dot{\mathsf{U}}(t)\|_0^2 + |\mathsf{U}(t)|_{\mathrm{dG}}^2 + |\mathsf{U}(t)|_{\Gamma_I}^2 + \int_0^t \mathcal{D}(\dot{\mathsf{U}}, \dot{\mathsf{U}})(s)\, ds + \mathcal{D}(\mathsf{U}, \mathsf{U})(0),$$

for all $\mathsf{U} = (\boldsymbol{u}_e, \boldsymbol{u}_p, \boldsymbol{u}_f) \in C^1([0, T]; \boldsymbol{V}_h)$, where

$$|\mathsf{U}|_{\mathrm{dG}}^2 = \|\boldsymbol{u}_e(t)\|_{\mathrm{dG,e}}^2 + \|\boldsymbol{u}_p(t)\|_{\mathrm{dG,p}}^2 + |(\beta\boldsymbol{u}_p + \boldsymbol{u}_f)(t)|_{\mathrm{dG,p}}^2,$$
$$\|\boldsymbol{u}_\star\|_{\mathrm{dG,\star}}^2 = \|\mathbb{C}^{1/2} : \boldsymbol{\epsilon}_h(\boldsymbol{u}_\star)\|_{\Omega_\star}^2 + \|\alpha^{1/2}[\![\boldsymbol{u}_\star]\!]\|_{\mathcal{F}_h^\star}^2 \qquad\qquad \forall \boldsymbol{u}_\star \in \boldsymbol{V}_h^\star \ \star = \{e, p\},$$

$$|\boldsymbol{u}_p|^2_{\mathrm{dG,p}} = \|m^{1/2}\nabla_h \cdot \boldsymbol{u}_p\|^2_{\Omega_p} + \|\gamma^{1/2}[\![\boldsymbol{u}_p]\!]_{\boldsymbol{n}}\|^2_{\mathcal{F}^p_h} \qquad\qquad \forall \boldsymbol{u}_p \in \boldsymbol{V}^p_h,$$

and for any $(\boldsymbol{u}_e, \boldsymbol{u}_p, \boldsymbol{u}_f) \in \boldsymbol{V}^e_h \times \boldsymbol{V}^p_h \times \boldsymbol{V}^p_h$ we have

$$|\mathsf{U}|^2_{\Gamma_I} = \|\alpha^{1/2}(\boldsymbol{u}_p - \boldsymbol{u}_e)\|^2_{\mathcal{F}^I_h} + \|\gamma^{1/2}((1-\delta)\beta\boldsymbol{u}_p + \boldsymbol{u}_f)\cdot\boldsymbol{n}_p\|^2_{\mathcal{F}^I_h}.$$

Before showing the main result of the section, we introduce the following fundamental lemmas.

LEMMA 3.3. *For any* $\mathsf{U}, \mathsf{V} \in \boldsymbol{V}_h$ *and for large enough parameters* c_1, c_2, *it holds*

$$\mathcal{A}_h(\mathsf{U}, \mathsf{U}) \gtrsim |\mathsf{U}|^2_{\mathrm{dG}}, \qquad\qquad \mathcal{A}_h(\mathsf{U}, \mathsf{V}) \lesssim |\mathsf{U}|_{\mathrm{dG}}|\mathsf{V}|_{\mathrm{dG}}.$$

Proof. For the proof we use the definition of the bilinear form $\mathcal{A}_h(\cdot,\cdot)$ in (3.3) and combine the results in [9, Lemma A.3]. □

LEMMA 3.4. *For any* $(\boldsymbol{u}_e, \boldsymbol{u}_p) \in \boldsymbol{V}^e_h \times \boldsymbol{V}^p_h$ *and any* $\boldsymbol{u}_f \in \boldsymbol{V}^p_h$ *it holds*

$$(3.11) \qquad 2|\langle \boldsymbol{\sigma}_{eh}(\boldsymbol{u}_e)\boldsymbol{n}_e, \boldsymbol{u}_p - \boldsymbol{u}_e\rangle_{\mathcal{F}^I_h}| \lesssim \frac{1}{\sqrt{c_1}}\|\boldsymbol{u}_e\|_{\mathrm{dG,e}}\|\alpha^{1/2}(\boldsymbol{u}_p - \boldsymbol{u}_e)\|_{\mathcal{F}^I_h},$$

$$(3.12) \quad 2|\langle m\nabla\cdot(\beta\boldsymbol{u}_p + \boldsymbol{u}_f), ((1-\delta)\beta\boldsymbol{u}_p + \boldsymbol{u}_f)\cdot\boldsymbol{n}_p\rangle_{\mathcal{F}^I_h}|$$
$$\lesssim \frac{1}{\sqrt{c_2}}|(\beta\boldsymbol{u}_p + \boldsymbol{u}_f)(t)|_{\mathrm{dG,p}}\|\gamma^{1/2}((1-\delta)\beta\boldsymbol{u}_p + \boldsymbol{u}_f)\cdot\boldsymbol{n}_p\|_{\mathcal{F}^I_h},$$

where c_1 *and* c_2 *are the two positive constants at our disposal appearing in the definition of the stabilization function given in* (3.5)–(3.6).

Proof. The proof hinges on Assumption 3.1 and the trace inverse inequality (3.1). See also [9, Lemma A.2] □

COROLLARY 3.5. *For any* $\mathsf{U} = (\boldsymbol{u}_e, \boldsymbol{u}_p, \boldsymbol{u}_f) \in \boldsymbol{V}_h$ *and for* c_1 *and* c_2 *large enough it holds*

$$(3.13) \qquad |\mathsf{U}|^2_{\mathrm{dG}} + |\mathsf{U}|^2_{\Gamma_I} \lesssim \mathcal{A}_h(\mathsf{U}, \mathsf{U}) + \mathcal{C}_h(\mathsf{U}, \mathsf{U}) \lesssim |\mathsf{U}|^2_{\mathrm{dG}} + |\mathsf{U}|^2_{\Gamma_I}.$$

Proof. The proof follows by noting that

$$\mathcal{C}_h(\mathsf{U}, \mathsf{W}) = -2\langle\boldsymbol{\sigma}_e(\boldsymbol{u}_e)\boldsymbol{n}_p, \boldsymbol{u}_p - \boldsymbol{u}_e\rangle_{\mathcal{F}^I_h} - 2\langle m\nabla\cdot(\beta\boldsymbol{u}_p + \boldsymbol{u}_f), ((1-\delta)\beta\boldsymbol{u}_p + \boldsymbol{u}_f)\cdot\boldsymbol{n}_p\rangle_{\Gamma_I}$$
$$+ \|\alpha^{1/2}(\boldsymbol{u}_p - \boldsymbol{u}_f)\|^2_{\mathcal{F}^I_h} + \|\gamma^{1/2}((1-\delta)\beta\boldsymbol{u}_p + \boldsymbol{u}_f)\cdot\boldsymbol{n}_p\|^2_{\mathcal{F}^I_h},$$

and using the results in Lemma 3.3 and Lemma 3.4. □

The main stability result is stated in the following theorem.

THEOREM 3.6 (Stability of the semi-discrete formulation). *Let* Assumption 3.1 *and* Assumption 3.2 *be satisfied. For sufficiently large penalty parameters* c_1 *and* c_2 *in* (3.5) *and* (3.6), *respectively, let* $\mathsf{U}_h(t) \in \boldsymbol{V}_h$ *be the solution of* (3.2) *for any* $t \in (0, T]$. *Then, it holds*

$$(3.14) \qquad \sup_{0 \leq t \leq T}\|\mathsf{U}_h(t)\|^2_{\mathrm{E}} \lesssim \|\mathsf{U}_{h0}\|^2_{\mathrm{E}} + \int_0^T\left(\|(2\rho_e\zeta)^{-1/2}\boldsymbol{f}_e\|^2_{\Omega_e} + \|(2\rho_e\zeta)^{-1/2}\boldsymbol{f}_p\|^2_{\Omega_p}\right.$$
$$\left. + \|(k/\eta)^{1/2}\boldsymbol{g}_p\|^2_{\Omega_p}\right)ds,$$

where the hidden constant depends on the final time T, *on the penalization parameters* c_1 *and* c_2 *in* (3.5)–(3.6) *and on the material properties.*

Proof. By taking $\mathsf{V}_h = \dot{\mathsf{U}}_h \in \boldsymbol{V}_h$ in (3.2) we obtain

$$\frac{1}{2}\frac{d}{dt}\left[\mathcal{M}(\dot{\mathsf{U}}_h, \dot{\mathsf{U}}_h) + \mathcal{A}_h(\mathsf{U}_h, \mathsf{U}_h) + \mathcal{C}_h(\mathsf{U}_h, \mathsf{U}_h)\right] + \mathcal{D}(\dot{\mathsf{U}}_h, \dot{\mathsf{U}}_h) = \mathcal{F}(\dot{\mathsf{U}}_h).$$

Next, we integrate in time between 0 and t, add on both side $\mathcal{D}(\mathsf{U}_0, \mathsf{U}_0) \geq 0$, use (3.13) and (2.10)–(2.11) to obtain

$$\|\mathsf{U}_h(t)\|_{\mathrm{E}}^2 + \int_0^t \mathcal{D}(\dot{\mathsf{U}}_h, \dot{\mathsf{U}}_h)(s)\,ds \lesssim \|\mathsf{U}_{h0}\|_{\mathrm{E}}^2 + 2\int_0^t \mathcal{F}(\dot{\mathsf{U}}_h)(s)\,ds,$$

for large enough penalty constants c_1 and c_2. Next, to estimate the last term on the right-hand side we use the Cauchy-Schwarz and Young inequalities. □

4. Semi-discrete error analysis. This section is devoted to the semi-discrete error analysis. We first recall some standard interpolation error estimates written in the context of polytopal discretizations and then present the main results of the section. We introduce the following definition and a further mesh assumption (cf. [30, 29]) in order to avoid technicalities in the following proofs.

DEFINITION 4.1. *A covering $\mathcal{T}_\S = \{\mathcal{K}\}$ of the polytopic mesh $\mathcal{T}_h$ is a set of regular shaped d-dimensional simplices $\mathcal{K}$, $d = 2, 3$, s.t. $\forall\ \kappa \in \mathcal{T}_h$, $\exists\ \mathcal{K} \in \mathcal{T}_\S$ s.t. $\kappa \subseteq \mathcal{K}$.*

ASSUMPTION 4.1. *Any mesh $\mathcal{T}_h$ admits a covering $\mathcal{T}_\S$ in the sense of Definition 4.1 such that i) $\max_{\kappa \in \mathcal{T}_h} card\{\kappa' \in \mathcal{T}_h : \kappa' \cap \mathcal{K} \neq \emptyset,\ \mathcal{K} \in \mathcal{T}_\S\ s.t.\ \kappa \subset \mathcal{K}\} \lesssim 1$ and ii) $h_\mathcal{K} \lesssim h_\kappa$ for each pair $\kappa \in \mathcal{T}_h$, $\mathcal{K} \in \mathcal{T}_\S$ with $\kappa \subset \mathcal{K}$.*

For all $t \in [0, T]$ we also introduce the norm

$$\|\mathsf{U}(t)\|_{\mathrm{E}}^2 = \|\dot{\mathsf{U}}(t)\|_0^2 + \|\mathsf{U}(t)\|_{\mathrm{dG}}^2 + |\mathsf{U}(t)|_{\Gamma_I}^2 + \int_0^t \mathcal{D}(\dot{\mathsf{U}}, \dot{\mathsf{U}})(s)\,ds + \mathcal{D}(\mathsf{U}, \mathsf{U})(0),$$

for any $\mathsf{U} = (\boldsymbol{u}_e, \boldsymbol{u}_p, \boldsymbol{u}_f) \in \boldsymbol{H}^2(\mathcal{T}_h^e) \times \boldsymbol{H}^2(\mathcal{T}_h^p) \times \boldsymbol{H}^2(\mathcal{T}_h^p)$, where

$$(4.1) \quad \|\mathsf{U}\|_{\mathrm{dG}}^2 = |\mathsf{U}|_{\mathrm{dG}}^2 + \|\alpha^{-1/2}\{\mathbb{C} : \boldsymbol{\epsilon}_h(\boldsymbol{u}_e)\}\|_{\mathcal{F}_h^e}^2 + \|\alpha^{-1/2}\{\mathbb{C} : \boldsymbol{\epsilon}_h(\boldsymbol{u}_p)\}\|_{\mathcal{F}_h^p}^2$$
$$+ \|\gamma^{-1/2}\{m\nabla_h \cdot (\beta\boldsymbol{u}_p + \boldsymbol{u}_f)\}\|_{\mathcal{F}_h^p}^2.$$

Next, we prove the following lemma.

LEMMA 4.2. *For any $\mathsf{U} \in \boldsymbol{H}^2(\mathcal{T}_h^e) \times \boldsymbol{H}^2(\mathcal{T}_h^p) \times \boldsymbol{H}^2(\mathcal{T}_h^p)$ and any $\mathsf{V}_h \in \boldsymbol{V}_h$ it holds*

$$(4.2) \qquad \mathcal{A}_h(\mathsf{U}, \mathsf{V}_h) + \mathcal{C}_h(\mathsf{U}, \mathsf{V}_h) \lesssim (\|\mathsf{U}\|_{\mathrm{dG}} + |\mathsf{U}|_{\Gamma_I})(|\mathsf{V}_h|_{\mathrm{dG}} + |\mathsf{V}_h|_{\Gamma_I}).$$

Proof. The proof is obtained by using classical dG arguments and by noting that

$$\mathcal{C}_h(\mathsf{U}, \mathsf{V}_h) = -\langle \boldsymbol{\sigma}_{eh}(\boldsymbol{u}_e)\boldsymbol{n}_p, \boldsymbol{v}_{ph} - \boldsymbol{v}_{eh}\rangle_{\mathcal{F}_h^I} - \langle \boldsymbol{\sigma}_{eh}(\boldsymbol{v}_{eh})\boldsymbol{n}_p, \boldsymbol{u}_p - \boldsymbol{u}_e\rangle_{\mathcal{F}_h^I}$$
$$+ \langle \alpha(\boldsymbol{u}_p - \boldsymbol{u}_e), \boldsymbol{v}_{ph} - \boldsymbol{v}_{eh}\rangle_{\mathcal{F}_h^I}$$
$$- \langle m\nabla_h \cdot (\beta\boldsymbol{u}_p + \boldsymbol{u}_f), ((1-\delta)\beta\boldsymbol{v}_{ph} + \boldsymbol{v}_{fh}) \cdot \boldsymbol{n}_p\rangle_{\mathcal{F}_h^I}$$
$$- \langle m\nabla_h \cdot (\beta\boldsymbol{v}_{ph} + \boldsymbol{v}_{fh}), ((1-\delta)\beta\boldsymbol{u}_p + \boldsymbol{u}_f) \cdot \boldsymbol{n}_p\rangle_{\mathcal{F}_h^I}$$
$$+ \langle \gamma((1-\delta)\beta\boldsymbol{u}_p + \boldsymbol{u}_f) \cdot \boldsymbol{n}_p, ((1-\delta)\beta\boldsymbol{v}_{ph} + \boldsymbol{v}_{fh}) \cdot \boldsymbol{n}_p\rangle_{\mathcal{F}_h^I}.$$

See also [13] and [9, Lemma A.3]. □

For an open bounded polytopic domain $\Sigma \subset \mathbb{R}^d$ and a generic polytopic mesh $\mathcal{T}_h$ over Σ satisfying Assumption 4.1, as in [30], we can introduce the Stein's extension operator $\tilde{\mathcal{E}} : H^m(\kappa) \to H^m(\mathbb{R}^d)$ [72], for any $\kappa \in \mathcal{T}_h$ and $m \in \mathbb{N}_0$, such that $\tilde{\mathcal{E}}v|_\kappa = v$ and $\|\tilde{\mathcal{E}}v\|_{m,\mathbb{R}^d} \lesssim \|v\|_{m,\kappa}$. The corresponding vector-valued version mapping $\boldsymbol{H}^m(\kappa)$ onto $\boldsymbol{H}^m(\mathbb{R}^d)$ acts component-wise and is denoted in the same way. In what follows, for any $\kappa \in \mathcal{T}_h$, we will denote by $\mathcal{K}_\kappa$ the simplex belonging to $\mathcal{T}_\S$ such that $\kappa \subset \mathcal{K}_\kappa$.

The next result provides the interpolation bounds that are instrumental for the derivation of the a-priori error estimate.

LEMMA 4.3. *For any* $\mathsf{U} = (\boldsymbol{u}_e, \boldsymbol{u}_p, \boldsymbol{u}_f) \in C^1([0,T]; \boldsymbol{V} \cap \boldsymbol{H}^m(\mathcal{T}_h^e) \times \boldsymbol{H}^n(\mathcal{T}_h^p) \times \boldsymbol{H}^\ell(\mathcal{T}_h^p))$ *with* $m, n, \ell \geq 2$, *there exists* $\mathsf{U}_I = (\boldsymbol{u}_e, \boldsymbol{u}_p, \boldsymbol{u}_f)_I \in C^1([0,T]; \boldsymbol{V}_h)$ *such that*

(4.3)
$$\max_{0 \leq t \leq T} \|\|(\mathsf{U} - \mathsf{U}_I)(t)\|\|_{\mathrm{E}}^2 \lesssim \sum_{\kappa \in \mathcal{T}_h^e} \frac{h_\kappa^{2(s_\kappa - 1)}}{p_{e,\kappa}^{2m-3}} \mathcal{N}(\boldsymbol{u}_e)_{m,\mathcal{K}_\kappa}^2 + \sum_{\kappa \in \mathcal{T}_h^p} \frac{h_\kappa^{2(q_\kappa - 1)}}{p_{p,\kappa}^{2n-3}} \mathcal{N}(\boldsymbol{u}_p)_{n,\mathcal{K}_\kappa}^2$$
$$+ \sum_{\kappa \in \mathcal{T}_h^p} \frac{h_\kappa^{2(r_\kappa - 1)}}{p_{p,\kappa}^{2\ell-3}} \mathcal{N}(\boldsymbol{u}_f)_{\ell,\mathcal{K}_\kappa}^2,$$

where $s_\kappa = \min(m, p_{e,\kappa} + 1)$, $q_\kappa = \min(n, p_{p,\kappa} + 1)$, $r_\kappa = \min(\ell, p_{p,\kappa} + 1)$, *and*

$$\mathcal{N}(\boldsymbol{u})_{m,\mathcal{K}_\kappa}^2 = \max_{0 \leq t \leq T} \left((1+T) \|\tilde{\mathcal{E}}\dot{\boldsymbol{u}}(t)\|_{m,\mathcal{K}_\kappa}^2 + \|\tilde{\mathcal{E}}\boldsymbol{u}(t)\|_{m,\mathcal{K}_\kappa}^2 \right).$$

Proof. The first part of the proof readily follows by reasoning as in [5, Lemma 5.1], cf. also [9, Lemma 4.2]. To infer estimate (4.3), we resort to the *hp*-approximation properties stated in [29, Lemma 23], implying

$$\|\dot{\mathsf{U}} - \dot{\mathsf{U}}_I\|_0^2 \lesssim \sum_{\kappa \in \mathcal{T}_h^e} \frac{h_\kappa^{2s_\kappa}}{p_{e,\kappa}^{2m}} \|\tilde{\mathcal{E}}\dot{\boldsymbol{u}}_e\|_{m,\mathcal{K}_\kappa}^2 + \sum_{\kappa \in \mathcal{T}_h^p} \frac{h_\kappa^{2q_\kappa}}{p_{p,\kappa}^{2n}} \|\tilde{\mathcal{E}}\dot{\boldsymbol{u}}_p\|_{n,\mathcal{K}_\kappa}^2 + \sum_{\kappa \in \mathcal{T}_h^p} \frac{h_\kappa^{2r_\kappa}}{p_{p,\kappa}^{2\ell}} \|\tilde{\mathcal{E}}\dot{\boldsymbol{u}}_f\|_{\ell,\mathcal{K}_\kappa}^2.$$

Then, a similar result hods for the terms $\int_0^t \mathcal{D}(\dot{\mathsf{U}} - \dot{\mathsf{U}}_I, \dot{\mathsf{U}} - \dot{\mathsf{U}}_I)(s)\, ds$ and $\mathcal{D}(\mathsf{U} - \mathsf{U}_I, \mathsf{U} - \mathsf{U}_I)(0)$. Finally, we bound the term $|\mathsf{U} - \mathsf{U}_I)|_{\Gamma_I}^2$ by applying the triangle and Cauchy–Schwarz inequalities followed by [29, Lemma 33], to infer

$$|\mathsf{U} - \mathsf{U}_I|_{\Gamma_I}^2 \lesssim \|\alpha^{1/2}(\boldsymbol{u}_e - \boldsymbol{u}_{eI})\|_{\mathcal{F}_h^I}^2 + \|\alpha^{1/2}(\boldsymbol{u}_p - \boldsymbol{u}_{pI})\|_{\mathcal{F}_h^I}^2$$
$$+ \|\gamma^{1/2}(1-\delta)\beta(\boldsymbol{u}_p - \boldsymbol{u}_{pI}) \cdot \boldsymbol{n}_p\|_{\mathcal{F}_h^I}^2 + \|\gamma^{1/2}(\boldsymbol{u}_f - \boldsymbol{u}_{fI}) \cdot \boldsymbol{n}_p\|_{\mathcal{F}_h^I}^2$$
$$\lesssim \sum_{\kappa \in \mathcal{T}_h^e} \frac{h_\kappa^{2(s_\kappa - 1)}}{p_{e,\kappa}^{2m-3}} \|\tilde{\mathcal{E}}\boldsymbol{u}_e\|_{m,\mathcal{K}_\kappa}^2 + \sum_{\kappa \in \mathcal{T}_h^p} \frac{h_\kappa^{2(q_\kappa - 1)}}{p_{p,\kappa}^{2n-3}} \|\tilde{\mathcal{E}}\boldsymbol{u}_p\|_{n,\mathcal{K}_\kappa}^2$$
$$+ \sum_{\kappa \in \mathcal{T}_h^p} \frac{h_\kappa^{2(r_\kappa - 1)}}{p_{p,\kappa}^{2\ell-3}} \|\tilde{\mathcal{E}}\boldsymbol{u}_f\|_{\ell,\mathcal{K}_\kappa}^2. \qquad \square$$

Before presenting the main result of this Section, we set for any time $t \in (0,T]$

$$\mathsf{E}(t) = (\mathsf{U} - \mathsf{U}_h)(t) = (\boldsymbol{u}_e - \boldsymbol{u}_{eh}, \boldsymbol{u}_p - \boldsymbol{u}_{ph}, \boldsymbol{w}_p - \boldsymbol{w}_{ph})(t),$$

and use the *strong consistency* of the semi-discrete formulation (3.2) to write the following *error equation*

(4.4) $$\mathcal{M}(\ddot{\mathsf{E}}, \mathsf{V}_h) + \mathcal{D}(\dot{\mathsf{E}}, \mathsf{V}_h) + \mathcal{A}_h(\mathsf{E}, \mathsf{V}_h) + \mathcal{C}_h(\mathsf{E}, \mathsf{V}_h) = 0 \quad \forall \mathsf{V}_h \in \boldsymbol{V}_h.$$

THEOREM 4.4 (Semi-discrete error estimates). *Let* Assumption 3.1, *Assumption* 3.2, *Assumption* 4.1, *and the hypothesis of* Theorem 2.2 *hold. Let the solution* $\mathsf{U} = (\boldsymbol{u}_e, \boldsymbol{u}_p, \boldsymbol{u}_f)$ *of problem* (2.7) *be such that*

$$\mathsf{U} \in C^2([0,T]; \boldsymbol{H}^m(\mathcal{T}_h^e) \times \boldsymbol{H}^n(\mathcal{T}_h^p) \times \boldsymbol{H}^\ell(\mathcal{T}_h^p)) \cap C^1([0,T]; \boldsymbol{V}),$$

with $m, n, \ell \geq 2$ *and let* $\mathsf{U}_h = (\boldsymbol{u}_e, \boldsymbol{u}_p, \boldsymbol{u}_f)_h \in C^2([0,T]; \boldsymbol{V}_h)$ *be the solution of* (3.2) *with* c_1 *and* c_2 *sufficiently large. Then, the discretization error* $\mathsf{E} = \mathsf{U} - \mathsf{U}_h$ *satisfies*

$$(4.5) \quad \max_{0 \leq t \leq T} \|\mathsf{E}(t)\|_{\mathrm{E}}^2 \lesssim \sum_{\kappa \in \mathcal{T}_h^e} \frac{h_\kappa^{2(s_\kappa - 1)}}{p_{e,\kappa}^{2m-3}} \mathcal{N}(\boldsymbol{u}_e)_{m,\mathcal{K}_\kappa}^2 + \sum_{\kappa \in \mathcal{T}_h^p} \frac{h_\kappa^{2(q_\kappa - 1)}}{p_{p,\kappa}^{2n-2}} \mathcal{N}(\boldsymbol{u}_p)_{n,\mathcal{K}_\kappa}^2$$

$$+ \sum_{\kappa \in \mathcal{T}_h^p} \frac{h_\kappa^{2(r_\kappa - 1)}}{p_{p,\kappa}^{2\ell-3}} \mathcal{N}(\boldsymbol{u}_f)_{\ell,\mathcal{K}_\kappa}^2,$$

with $\mathcal{N}(\boldsymbol{u})_{m,\mathcal{K}_\kappa}^2 = \max_{0 \leq t \leq T} \left(\|\widetilde{\mathcal{E}} \ddot{\boldsymbol{u}}(t)\|_{m,\mathcal{K}_\kappa}^2 + \|\widetilde{\mathcal{E}} \dot{\boldsymbol{u}}(t)\|_{m,\mathcal{K}_\kappa}^2 + \|\widetilde{\mathcal{E}} \boldsymbol{u}(t)\|_{m,\mathcal{K}_\kappa}^2 \right)$ *and hidden constant depending on the final time* T *and the material properties, but independent of the discretization parameters.*

Proof. For any time $t \in (0, T]$, let $\mathsf{U}_I(t) = (\boldsymbol{u}_e, \boldsymbol{u}_p, \boldsymbol{u}_f)_I(t) \in \boldsymbol{V}_h$ be the interpolants defined in Lemma 4.3. We split the error as $\mathsf{E}(t) = \mathsf{E}_I(t) - \mathsf{E}_h(t)$, where

$$\mathsf{E}_I(t) = (\mathsf{U} - \mathsf{U}_I)(t) = (\boldsymbol{u}_e - \boldsymbol{u}_{eI}, \boldsymbol{u}_p - \boldsymbol{u}_{pI}, \boldsymbol{u}_f - \boldsymbol{u}_{fI})(t),$$
$$\mathsf{E}_h(t) = (\mathsf{U}_h - \mathsf{U}_I)(t) = (\boldsymbol{u}_{eh} - \boldsymbol{u}_{eI}, \boldsymbol{u}_{ph} - \boldsymbol{u}_{pI}, \boldsymbol{u}_{fh} - \boldsymbol{u}_{fI})(t).$$

From the triangle inequality, we have $\|\mathsf{E}(t)\|_{\mathrm{E}}^2 \leq \|\mathsf{E}_h(t)\|_{\mathrm{E}}^2 + \|\mathsf{E}_I(t)\|_{\mathrm{E}}^2$, and Lemma 4.3 can be used to bound the term $\|\mathsf{E}_I(t)\|_{\mathrm{E}}$. As for the term $\|\mathsf{E}_h(t)\|_{\mathrm{E}}$, by taking $\mathsf{V}_h = \dot{\mathsf{E}}_h \in \boldsymbol{V}_h$ as test functions in (4.4) and collecting a first time derivative, we obtain

$$(4.6) \quad \frac{1}{2} \frac{d}{dt} \left(\mathcal{M}(\dot{\mathsf{E}}_h, \dot{\mathsf{E}}_h) + \mathcal{A}_h(\mathsf{E}_h, \mathsf{E}_h) + \mathcal{C}_h(\mathsf{E}_h, \mathsf{E}_h) \right) + \mathcal{D}(\dot{\mathsf{E}}_h, \dot{\mathsf{E}}_h) = \mathcal{M}(\ddot{\mathsf{E}}_I, \dot{\mathsf{E}}_h)$$

$$+ \mathcal{D}(\dot{\mathsf{E}}_I, \dot{\mathsf{E}}_h) - \mathcal{A}_h(\dot{\mathsf{E}}_I, \mathsf{E}_h) - \mathcal{C}_h(\dot{\mathsf{E}}_I, \mathsf{E}_h) + \frac{d}{dt} \mathcal{A}_h(\mathsf{E}_I, \mathsf{E}_h) + \frac{d}{dt} \mathcal{C}_h(\mathsf{E}_I, \mathsf{E}_h),$$

where we have used Leibniz's rule on the term $\mathcal{A}_h(\mathsf{E}_I, \dot{\mathsf{E}}_h)$ and $\mathcal{C}_h(\mathsf{E}_I, \dot{\mathsf{E}}_h)$. Now, reasoning as in the proof of Theorem 3.6, integrating (4.6) between 0 and $t \leq T$, and assuming for simplicity that we can set the initial conditions of the semi-discrete problem so that $\dot{\mathsf{E}}_h(0) = \mathsf{E}_h(0) = \boldsymbol{0}$, we get

$$\|\mathsf{E}_h(t)\|_{\mathrm{E}}^2 + \int_0^t \mathcal{D}(\dot{\mathsf{E}}_h, \dot{\mathsf{E}}_h)(s) \, ds \lesssim \mathcal{A}_h(\mathsf{E}_I, \mathsf{E}_h)(t) + \mathcal{C}_h(\mathsf{E}_I, \mathsf{E}_h)(t)$$

$$+ \int_0^t \left(\mathcal{M}(\ddot{\mathsf{E}}_I, \dot{\mathsf{E}}_h) - \mathcal{A}_h(\dot{\mathsf{E}}_I, \mathsf{E}_h) - \mathcal{C}_{\Gamma_I}(\dot{\mathsf{E}}_I, \mathsf{E}_h) + \mathcal{D}(\dot{\mathsf{E}}_I, \dot{\mathsf{E}}_h) \right)(s) \, ds.$$

Note that also $\mathcal{D}(\mathsf{E}_h, \mathsf{E}_h)(0) = 0$ under the assumption that $\mathsf{U}_h(0) = \mathsf{U}_I(0)$. Then, we apply Cauchy-Schwarz and Young's inequality together with (4.2) to get

$$\|\mathsf{E}_h(t)\|_{\mathrm{E}}^2 \lesssim \|\|\mathsf{E}_I\|\|_{\mathrm{dG}}^2 + |\mathsf{E}_I|_{\Gamma_I}^2 + \int_0^t \mathcal{D}(\dot{\mathsf{E}}_I, \dot{\mathsf{E}}_I)(s) \, ds$$

$$+ \int_0^t (\|\ddot{\mathsf{E}}_I\|_0 + \|\|\dot{\mathsf{E}}_I\|\|_{\mathrm{dG}} + |\dot{\mathsf{E}}_I|_{\Gamma_I})(\|\dot{\mathsf{E}}_h\|_0 + \|\mathsf{E}_h\|_{\mathrm{dG}} + |\mathsf{E}_h|_{\Gamma_I})(s) \, ds.$$

We note that the first three addends can be bounded by $\||\mathsf{E}_I(t)\||_{\mathrm{E}}^2$. Finally, we take the maximum over $t \in [0, T]$, employ the Cauchy-Schwarz and Young's inequality, and observe that $\int_0^T |f(s)| ds \leq T \max_{t \in [0,T]} |f(t)|$ to infer

$$\max_{0 \leq t \leq T} \|\mathsf{E}_h(t)\|_{\mathrm{E}}^2 \lesssim \max_{0 \leq t \leq T} \||\mathsf{E}_I(t)\||_{\mathrm{E}}^2 + T^2 \max_{0 \leq t \leq T} (\|\ddot{\mathsf{E}}_I\|_0^2 + \||\mathsf{E}_I\||_{\mathrm{dG}}^2 + |\mathsf{E}_I|_{\Gamma_I}^2)(t)$$

$$\lesssim \max_{0 \leq t \leq T} \||\mathsf{E}_I(t)\||_{\mathrm{E}}^2 + T^2 \max_{0 \leq t \leq T} \||\dot{\mathsf{E}}_I(t)\||_{\mathrm{E}}^2.$$

We conclude by applying the estimates in Lemma 4.3. □

5. dG time discretization. It is known, in the literature, that problems of wave propagation in porous media present difficulties from the point of view of integration over time. This is because in the low-frequency range, as the one we are interested in, the evolution problem becomes stiff [33, 36], and therefore implicit time integration schemes might be preferred to avoid stability constraint. In that respect, to integrate in time the second-order differential system in (3.9) we adopt the scheme proposed in [14] for the elastodynamics equations, which consists in applying a time dG method to the first-order system

$$(5.1) \qquad \begin{bmatrix} I & 0 \\ 0 & M \end{bmatrix} \begin{bmatrix} \dot{\mathbf{U}}_h \\ \dot{\mathbf{V}}_h \end{bmatrix} + \begin{bmatrix} 0 & -I \\ A+C & D \end{bmatrix} \begin{bmatrix} \mathbf{U}_h \\ \mathbf{V}_h \end{bmatrix} = \begin{bmatrix} \mathbf{0} \\ \mathbf{F}_h \end{bmatrix}.$$

The latter can be rewritten in a compact form as

$$(5.2) \qquad \widehat{M} \dot{\mathbf{Z}}_h + \widehat{K} \mathbf{Z}_h = \widehat{\mathbf{F}}_h,$$

by setting $\mathbf{Z}_h = [\mathbf{U}_h, \mathbf{V}_h]^T$, and $\widehat{M}$ and $\widehat{K}$ defined as

$$\widehat{M} = \begin{bmatrix} I & 0 \\ 0 & M \end{bmatrix}, \quad \text{and} \quad \widehat{K} = \begin{bmatrix} 0 & -I \\ A+C & D \end{bmatrix}.$$

Remark that, with respect to the system introduced in [14], here the first equation of (5.1) has not been multiplied by A (that in this case is not positive definite). To discretize in time this system we partition the interval $I = (0, T]$ into N_T time-slabs $I_n = (t_{n-1}, t_n]$ having length $\Delta t_n = t_n - t_{n-1}$, for $n = 1, \ldots, N$ with $t_0 = 0$ and $t_N = T$. Then, we introduce the functional spaces

$$\boldsymbol{V}_{\Delta t_n}^{r_n} = \{\mathbf{Z} : I_n \to \mathbb{R}^{\mathsf{2ndof}} \text{ s.t. } \mathbf{Z} \in [\mathcal{P}^{r_n}(I_n)]^{\mathsf{2ndof}}, r_n \geq 1\},$$

and

$$(5.3) \qquad \boldsymbol{V}_{\Delta t}^r = \{\mathbf{Z} \in \boldsymbol{L}^2(0, T) \text{ s.t. } \mathbf{Z}|_{I_n} = [\mathbf{U}, \mathbf{V}]^T|_{I_n} \in \boldsymbol{V}_{\Delta t_n}^{r_n} \ \forall n = 1, ..., N_T\}.$$

We use the notation $[\cdot]_n$ to denote the jump of $\mathbf{Z} \in \boldsymbol{V}_{\Delta t}^r$ at time instant t_n, i.e., $[\mathbf{Z}]_n = \mathbf{Z}(t_n^+) - \mathbf{Z}(t_n^-)$, for $n \geq 0$. With this notation, the time-dG formulation of (5.2) reads as: find $\mathbf{Z}_{\mathrm{dG}} \in \boldsymbol{V}_{\Delta t}^r$ such that

$$(5.4) \qquad \mathcal{A}_{\mathrm{T}}(\mathbf{Z}_{\mathrm{dG}}, \mathbf{W}) = \mathcal{G}(\mathbf{W}) \qquad \forall \mathbf{W} \in \boldsymbol{V}_{\Delta t}^r,$$

where the bilinear form $\mathcal{A}_{\mathrm{T}} : \boldsymbol{V}_{\Delta t}^r \times \boldsymbol{V}_{\Delta t}^r \to \mathbb{R}$ is defined by

$$\mathcal{A}_{\mathrm{T}}(\mathbf{Z}, \mathbf{W}) = \sum_{n=1}^{N_T} (\widehat{M} \dot{\mathbf{Z}}, \mathbf{W})_{I_n} + (\widehat{K} \mathbf{Z}, \mathbf{W})_{I_n} + \sum_{n=1}^{N_T-1} \widehat{M} [\mathbf{Z}]_n \cdot \mathbf{W}(t_n^+) + \widehat{M} \mathbf{Z}(0^+) \cdot \mathbf{W}(0^+),$$

for all $\mathbf{Z}, \mathbf{W} \in \boldsymbol{V}_{\Delta t}^r$. The linear functional $\mathcal{G} : \boldsymbol{L}^2(0,T) \to \mathbb{R}$ is defined as

$$(5.5) \qquad \mathcal{G}(\mathbf{W}) = \sum_{n=1}^{N_T} (\widehat{\mathbf{F}}_h, \mathbf{W})_{I_n} + \widehat{M} \mathbf{Z}_0 \cdot \mathbf{W}(0^+),$$

for any $\mathbf{W} \in \boldsymbol{V}_{\Delta t}^r$, being $\mathbf{Z}_0 = [\mathbf{U}_{0h}, \mathbf{V}_{0h}]^T$. In practice, to compute the discrete solution to (5.4) we iterate over the time intervals, using as initial conditions for I_{n+1} the trace in t_n of the computed solution in the previous interval I_n. Hence, problem (5.4) written for the generic time interval I_n reduces to: find $\mathbf{Z}_{dG}^n \in \boldsymbol{V}_{\Delta t_n}^{r_n}$ such that

$$(5.6) \quad (\widehat{M}\dot{\mathbf{Z}}_{dG}^n, \mathbf{W})_{I_n} + (\widehat{K}\mathbf{Z}_{dG}^n, \mathbf{W})_{I_n} + \widehat{M}\mathbf{Z}_{dG}^n(t_{n-1}^+) \cdot \mathbf{W}(t_{n-1}^+)$$
$$= (\widehat{\mathbf{F}}_h, \mathbf{W})_{I_n} + \widehat{M}\mathbf{Z}_{dG}^{n-1}(t_{n-1}^-) \cdot \mathbf{W}(t_{n-1}^+).$$

Focusing on the generic interval I_n, we introduce a basis $\{\psi^\ell(t)\}^{\ell=1,\dots,r_n+1}$ for the polynomial space $\mathcal{P}^{r_n}(I_n)$ and set $\mathsf{d} = \mathsf{ndof}(r_n+1)$ the dimension of the local finite dimensional space $\boldsymbol{V}_{\Delta t_n}^{r_n}$. We also introduce the vectorial basis $\{\boldsymbol{\psi}_i^\ell(t)\}_{i=1,\dots,2\mathsf{ndof}}^{\ell=1,\dots,r_n+1}$, where $\boldsymbol{\psi}_i^\ell$ is the $2\mathsf{ndof}$-dimensional vector whose i-th component is ψ^ℓ and the other components are zero. Using the above notation, we can write the trial function Z_{dG}^n as a linear combination of the basis functions, i.e,

$$\mathbf{Z}_{dG}^n(t) = \sum_{j=1}^{2\mathsf{ndof}} \sum_{m=1}^{r_n+1} \alpha_j^m \boldsymbol{\psi}_j^m(t),$$

where $\alpha_j^m \in \mathbb{R}$ for $j = 1, \dots, 2\mathsf{ndof}$ and $m = 1, \dots, r_n+1$. Next, we write equation (5.6) for any test function $\boldsymbol{\psi}_i^\ell(t)$, $i = 1, \dots, 2\mathsf{ndof}$, $\ell = 1, \dots, r_n+1$, obtaining the algebraic system of equations

$$\boldsymbol{A}^n \boldsymbol{\alpha}^n = \boldsymbol{b}^n,$$

where on the interval I_n, $\boldsymbol{\alpha}^n \in \mathbb{R}^{2\mathsf{d}}$ is the solution vector, $\boldsymbol{b}^n \in \mathbb{R}^{2\mathsf{d}}$ corresponds to the data and is given componentwise as

$$\boldsymbol{b}_k^n = (\widehat{\mathbf{F}}_h, \boldsymbol{\psi}_i^\ell)_{I_n} + \widehat{M}\mathbf{Z}_{dG}^{n-1}(t_{n-1}^-)\boldsymbol{\psi}_i^\ell(t_{n-1}^+), \quad n = 1, \dots, N_T,$$

for $k = \ell + (i-1)(r_n+1)$, and $\ell = 1, \dots, r_n+1$, $i = 1, \dots, 2\mathsf{ndof}$. Note that we implicitly use the convention $\mathbf{Z}_{dG}^{n-1}(0^-) = \mathbf{Z}_{0h}$. The system matrix $\boldsymbol{A}^n \in \mathbb{R}^{2\mathsf{d} \times 2\mathsf{d}}$ has the following structure

$$\boldsymbol{A}^n = (N_1 + N_3) \otimes \begin{bmatrix} I & 0 \\ 0 & M \end{bmatrix} + N_2 \otimes \begin{bmatrix} 0 & -I \\ A+C & D \end{bmatrix}, \quad n = 1, \dots, N_T$$

where the time matrices N_i, $i = 1, 2, 3$, are defined as follows

$$N_1^{\ell m} = (\dot{\psi}^m, \psi^\ell)_{I_n}, \quad N_2^{\ell m} = (\psi^m, \psi^\ell)_{I_n}, \quad N_3^{\ell m} = \psi^m(t_{n-1}^+)\psi^\ell(t_{n-1}^+),$$

for $m, \ell = 1, \dots, r_n+1$. By defining the solution vector and the right-hand side $\boldsymbol{\alpha}^n = [\boldsymbol{\alpha}_u^n, \boldsymbol{\alpha}_v^n]^T$ and $\boldsymbol{b}^n = [\boldsymbol{b}_u^n, \boldsymbol{b}_v^n]^T$, respectively, and using the properties of the Kronecker product we obtain

$$(5.7) \qquad \left(I_n \otimes \begin{bmatrix} I & 0 \\ 0 & M \end{bmatrix} + N_5 \otimes \begin{bmatrix} 0 & -I \\ (A+C) & D \end{bmatrix} \right) \begin{bmatrix} \boldsymbol{\alpha}_u^n \\ \boldsymbol{\alpha}_w^n \end{bmatrix} = N_4 \otimes \begin{bmatrix} I & 0 \\ 0 & I \end{bmatrix} \begin{bmatrix} \boldsymbol{b}_u^n \\ \boldsymbol{b}_w^n \end{bmatrix},$$

where $N_4 = (N_1 + N_3)^{-1}$, $N_5 = N_4 N_2$, and I_n is the identity matrix of order $r_n + 1$. As noted in [69, Remark 1] the above scheme is equivalent to an Implicit Runge-Kutta (IRK) method with $(r_n + 1)$-stages. As in this case, when the entries of the time matrices N_i, $i = 1, .., 3$, and of the right-hand side are computed through a Gauss-Legendre-Lobatto (GLL) quadrature formula having $r_n + 1$ points and weights, and the basis functions ψ^ℓ are the characteristic polynomials associated with that points, one obtains the so-called IRK-Lobatto IIIC schemes (see, e.g. [66, Section 11.8.3]). As a consequence, scheme (5.7) is L-stable, algebraically stable, and thus B-stable. Moreover, as observed in [51], it is perfectly suited for stiff problems. According to [25] Lobatto IIIC methods with $r_n + 1$ stages have a maximal order of convergence $2r_n - 2$ when a scalar problem is taken into account. However, when the method is applied to a system of ordinary differential equations its order of accuracy can deteriorate as observed in [66, 69]. In the case under consideration it holds

$$\|\mathbf{Z}_h(T^-) - \mathbf{Z}_{\mathrm{dG}}(T^-)\|_2 \lesssim \Delta t^{r_n + 1},$$

if the time slabs I_n have all the same length Δt for any $n = 1, ..., N$, cf. Section 6. The formal proof of this result is out of the scope of the paper and will be subject to future research.

To numerically solve system (5.7) we apply a block Gaussian elimination getting

$$(5.8) \qquad \begin{bmatrix} I_n \otimes I & -N_5 \otimes I \\ 0 & M_w \end{bmatrix} \begin{bmatrix} \boldsymbol{\alpha}_u^n \\ \boldsymbol{\alpha}_w^n \end{bmatrix} = \begin{bmatrix} (N_4 \otimes I)\boldsymbol{b}_u^n \\ \boldsymbol{b}_w^n - (N_6 \otimes I)\boldsymbol{b}_u^n \end{bmatrix},$$

with $M_w = (N_1 + N_3) \otimes M + N_2 \otimes D + N_7 \otimes (A + C)$ being $N_6 = N_2 N_4$ and $N_7 = N_2 N_4 N_2$. Next, we compute $\boldsymbol{\alpha}_w^n$, by solving the linear system $M_w \boldsymbol{\alpha}_w^n = \boldsymbol{b}_w^n - (N_6 \otimes I)\boldsymbol{b}_u^n$ and then we update $\boldsymbol{\alpha}_u^n$ by using the first equation.

6. Numerical results.

In this section, we present numerical results concerning the verification of our scheme on problems with manufactured solutions and the application of the method to cases of geophysical interest. In all numerical tests, the penalty parameters c_1 and c_2 appearing in definitions (3.5)–(3.6), respectively, have been chosen equal to 10.

6.1. Verification test.

We consider problem (2.1)–(2.2) coupled with (2.4)–(2.6) in $\Omega = \Omega_e \cup \Omega_p$ with $\Omega_e = (0, 1) \times (0, 1)$ and $\Omega_p = (-1, 0) \times (0, 1)$. We choose the exact solution

$$(6.1) \qquad \boldsymbol{u}_e = \cos(4\pi t) \begin{bmatrix} x^2 \sin(2\pi x) \\ x^2 \sin(4\pi x) \end{bmatrix}, \quad \boldsymbol{u}_p = \cos(\pi\sqrt{2}t) \begin{bmatrix} x^2 \cos(\pi x/2) \sin(\pi x) \\ x^2 \cos(\pi x/2) \sin(\pi x) \end{bmatrix},$$

and $\boldsymbol{u}_f = -\boldsymbol{u}_p$. Dirichlet boundary conditions, initial conditions, and the forcing term $\boldsymbol{f}_e$, $\boldsymbol{f}_p$, and $\boldsymbol{g}_p$ are set accordingly. For the interface conditions (2.4)–(2.6) we choose $\delta = 1$. The model problem is solved on a sequence of polygonal meshes as the one shown in Figure 2, with adimensional parameters reported in Table 1.
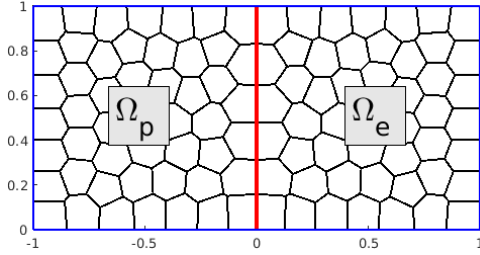
Fig. 2: Test case of Section 6.1. Example of the computational domain having 100 polygonal elements. The red line represents the interface Γ_I.

		Ω_p	Ω_e
Fluid	ρ_f	1	–
	η	1	–
Grain	$\rho_s\ (\rho_e)$	1	1
	μ	1	1
	ζ	1	1
Matrix	ϕ	0.5	–
	a	1	–
	k	1	–
	λ	1	2
	m	1	–
	β	1	–

Table 1: Parameters employed for the test case of Section 6.1.

As a first test, we set the final time equal to 1 and consider, for the time integration scheme in Section 5, a timestep $\Delta t_n = \Delta t = 10^{-3}$ and a polynomial degree $r_n = r = 1$, for any $n = 1, ..., 1000$. In Figure 3 (left), we report the computed energy error $\|\mathsf{U} - \mathsf{U}_h\|_{\mathrm{E}}$ at the final time T, cf. (3.10) as a function of the mesh size h for a polynomial degree $p_e = p_p = 2, 3, 4$. In this case, we retrieve the rate of convergence $\mathcal{O}(h^p)$ as proved in (4.5). In Figure 3 (right) we report the same results as before as a function of the polynomial degree $p = p_p = p_e$ obtained by fixing the number of grid elements $N_{el} = 100$ and considering $\Delta t_n = \Delta t = 5.e - 4$ and $r_n = r = 1$ for $n = 1, ..., 2000$. Notice that this latter case is not covered by our theoretical analysis, nevertheless, we observe numerically optimal convergence.

On the same numerical example, we compute numerically the L^2-norm of the error, i.e., $\|\mathbf{U} - \mathbf{U}_h\|_0$, as a function of the time step Δt, by fixing a polygonal mesh of $N_{el} = 100$ elements and the polynomial degree $p = p_p = p_e = 7$. We compute the error at the final time $T = 1$ by choosing different polynomial degrees $r = 1, 2, 3$. As it can be seen from Figure 4 the estimated order of convergence is $\mathcal{O}(\Delta t^r)$. Although this is only numerical evidence, it shows that the considered dG method outperforms classical methods such as the Newmark scheme, which is still widely used for wave propagation problems, see e.g., [9]. Next, in Table 2 we report the computed L^2-error $\|\mathbf{U} - \mathbf{U}_h\|_0$ as a function of the discretization parameters. In particular, we fix the polynomial degree for both space and time variables and we let N_{el} and Δt vary. It is possible to notice that the spatial discretization error is dominant since we obtain an almost constant value for each row of Table 2. It is interesting to analyze these results in connection with the condition number of the system matrix M_w, cf. Figure 5 (first row) and the computational time spent for the single run, cf. Figure 5 (second row). First of all, we can observe that the condition number of the system matrix increases by one order whenever the polynomial degree increases by one. Moreover, when fixing the polynomial degree, the matrix M_w is better conditioned for a smaller value of Δt, see Figure 5 (first row). Concerning the computational cost, it is obvious that this is proportional to the dimension of the system matrix. Looking at the plot in Figure 5 (second row) one can observe that even if different combinations of discretization parameters can lead to the same amount of time spent for a single simulation, they do not provide the same level of accuracy. Indeed, the sets ($p = r = 3, \Delta t = 0.01$, $N_{el} = 400$) and ($p = r = 4, \Delta t = 0.02, N_{el} = 200$) are equivalent from the point of
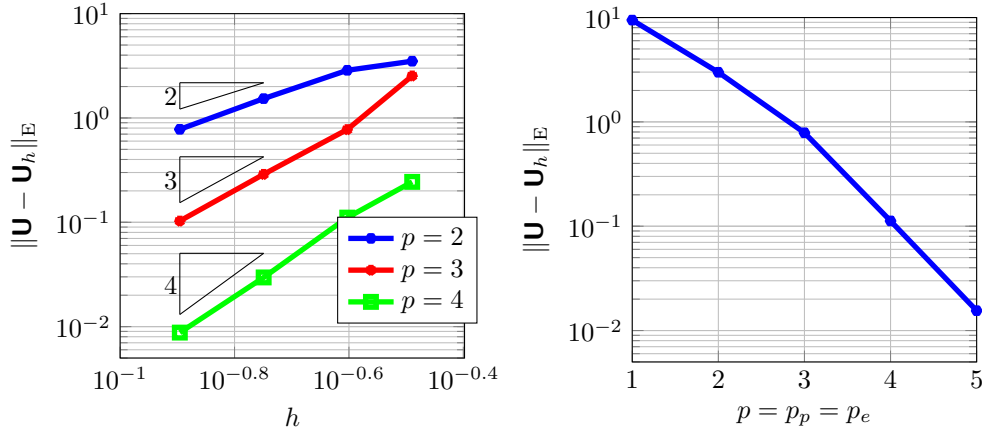
Fig. 3: Test case of Section 6.1. Left: computed energy-errors $\|\mathbf{U} - \mathbf{U}_h\|_{\mathrm{E}}$ at $T = 1$ in logarithmic scale as a function of the mesh size h for different polynomial degrees $p = p_e = p_p$ and fixing the time step $\Delta t = 0.001$ and the time polynomial degree $r = 1$. The rate of convergence is in agreement with the theoretical estimates in (4.5). Right: computed energy-errors $\|\mathbf{U} - \mathbf{U}_h\|_{\mathrm{E}}$ at $T = 1$ in semilogarithmic scale as a function of the polynomial degree $p = p_p = p_e$ by fixing the number of elements $N_{el} = 100$, the time step $\Delta t = 5.e - 4$, and the time polynomial degree $r = 1$.
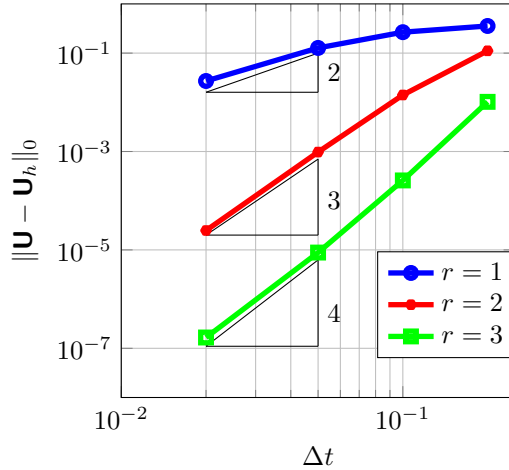
Fig. 4: Test case of Section 6.1. Computed L^2-errors $\|\mathbf{U} - \mathbf{U}_h\|_0$ at $T = 1$ in logarithmic scale as a function of the time step Δt for different polynomial degrees $r = 1, 2, 3$ in time. We set $N_{el} = 100$ polygonal elements and a space polynomial degree $p = p_p = p_e = 7$.

view of the computational cost (1389 s and 1130 s, respectively) but, with the first set we obtain an L^2-error equal to 1.7814e-04, while with the second we get 5.6899e-05.

6.2. Wave propagation in a two layer medium. Inspired by [60], we consider a wave propagation problem in a two-layered medium. The computational do-

$N_{el} \setminus \Delta t$		0.1	0.05	0.02	0.01
$p = r = 1$	50	2.5734e-01	2.3169e-01	2.1453e-01	2.0908e-01
	100	2.4613e-01	2.0702e-01	1.9284e-01	1.9759e-01
	200	2.4419e-01	1.9706e-01	1.8611e-01	1.8736e-01
	400	2.5188e-01	2.0336e-01	1.7338e-01	1.6802e-01
$p = r = 2$	50	4.8538e-02	4.8105e-02	4.8164e-02	4.8125e-02
	100	5.1387e-02	4.7603e-02	4.7353e-02	4.7406e-02
	200	3.2140e-02	2.7143e-02	2.6818e-02	2.6841e-02
	400	1.5432e-02	8.3925e-03	8.0168e-03	8.0096e-03
$p = r = 3$	50	1.5983e-02	1.5933e-02	1.5947e-02	1.5943e-02
	100	3.1176e-03	3.0956e-03	3.1093e-03	3.1157e-03
	200	8.7709e-04	8.4075e-04	8.4631e-04	8.5067e-04
	400	2.7540e-04	1.7519e-04	1.7682e-04	1.7814e-04
$p = r = 4$	50	9.1399e-04	9.2689e-04	9.3522e-04	9.3748e-04
	100	2.8139e-04	2.8182e-04	2.8601e-04	2.8739e-04
	200	5.6281e-05	5.6095e-05	5.6899e-05	5.7177e-05
	400	1.3301e-05	1.0781e-05	1.0890e-05	1.1072e-05

Table 2: Test case of Section 6.1. Computed L^2-errors $\|\mathbf{U} - \mathbf{U}_h\|_0$ as function of the discretization parameters.
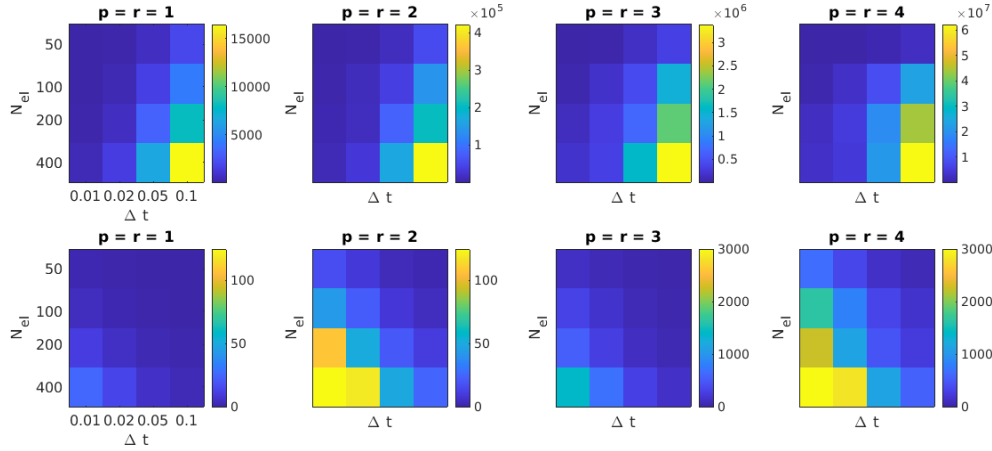
Fig. 5: Test case of Section 6.1. First row: computed condition number (`condest` function in Matlab) as a function of the discretization parameters. Second row: computational time employed for a single run as a function of the discretization parameters.

main $\Omega = (0, 4800\ m)^2$ and consists of two layers as shown in Figure 6 (left). We assume the upper layer to be a poroelastic material while the lower layer to be an elastic medium, cf. Table 3.

An explosive source is located in the upper layer at $\boldsymbol{x}_s = (1600, 2900)\ m$ whose
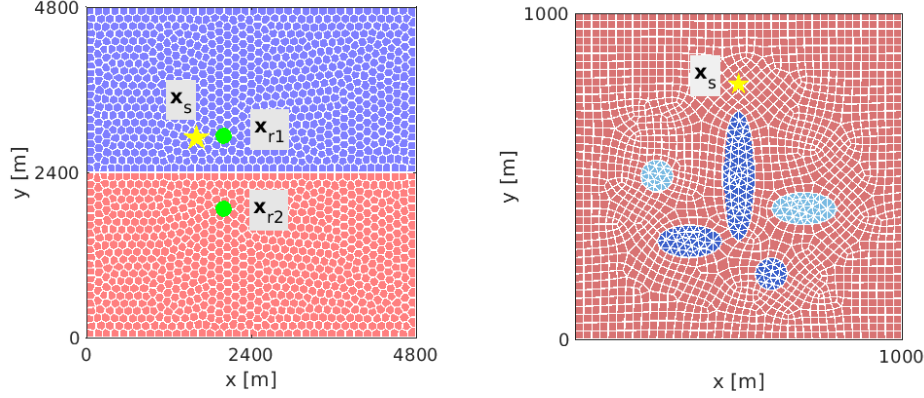
Fig. 6: Left: computational domain for the test case of Section 6.2. Right: computational domain for the test case of Section 6.3. Yellow stars denote the nucleation point $\boldsymbol{x}_s$, while green dots denotes the position of the receivers $\boldsymbol{x}_{r1}$ and $\boldsymbol{x}_{r2}$.

			Proelastic Layer	
Fluid	Fluid density	ρ_f	950	kg/m^3
	Dynamic viscosity	η	0 (0.0015)	Pa $\cdot$ s
Grain	Solid density	ρ_s	2200	kg/m^3
	Shear modulus	μ	4.3738 $\cdot 10^9$	Pa
Matrix	Porosity	ϕ	0.4	
	Tortuosity	a	2	
	Permeability	k	$1 \cdot 10^{-12}$	m^2
	Lamé coefficient	λ	7.2073$\cdot 10^9$	Pa
	Biot's coefficient	m	6.8386$\cdot 10^9$	Pa
	Biot's coefficient	β	0.0290	
	Damping coefficient	ζ	0 (0.01)	s^{-1}
			Elastic Layer	
Matrix	Solid density	ρ	2650	kg/m^3
	Shear modulus	μ	1.5038 $\cdot 10^9$	Pa
	Lamé coefficient	λ	1.8121$\cdot 10^9$	Pa
	Damping coefficient	ζ	0 (0.01)	s^{-1}

Table 3: Test case of Section 6.2. Physical parameters for the layered media.

expression is given by

$$(6.2) \qquad \boldsymbol{f}_p = \boldsymbol{g}_p = -M \cdot \nabla \delta(\boldsymbol{x} - \boldsymbol{x}_s) S(t),$$

being $M = M_0 I$ the moment tensor with $M_0 > 0$, $\delta(\boldsymbol{x} - \boldsymbol{x}_s)$ is the Dirac delta distribution centered in $\boldsymbol{x}_s$ and $S(t)$ is the source time function. This is a classical choice in the context of earthquake simulation, cf. [60]. We consider as a time evolution for $S(t)$ in (6.2) a Ricker-wavelet

$$(6.3) \qquad S(t) = (1 - 2\beta_p(t - t_0)^2)e^{-\beta_p(t-t_0)^2}, \quad \beta_p = \pi^2 f_p^2,$$

with time-shift $t_0 = 0.3$ s and peak-frequency $f_p = 5$ Hz. Finally, we set $M_0 = 1$ Nm. We use a shape-regular polygonal mesh with characteristic size $h = 100$ and a polynomial degree $p = 3$ for space discretization. For time integration, we set $\Delta t = 0.01$, a polynomial degree $r = 2$ and we fix the final time $T = 1.5$ s. For this model, we consider interface conditions (2.4)–(2.6) with $\delta = 1$, free surface boundary conditions on the top boundary, i.e. $\boldsymbol{\sigma}_p \boldsymbol{n}_p = \boldsymbol{0}$, and absorbing boundary conditions on the remaining part of the boundary to avoid artificial reflections and simulate an unbounded medium. In particular, we use the classical first-order paraxial approximations proposed in [71] for the elastic boundary Γ_e, i.e.,

$$(6.4) \qquad \boldsymbol{\sigma}_e \boldsymbol{n}_e = \rho_{(c_p - c_s)}(\partial_t \boldsymbol{u}_e \cdot \boldsymbol{n}_e)\boldsymbol{n}_e + \rho_e c_s \partial_t \boldsymbol{u}_e,$$

and the ones proposed in [60] for the poroelastic boundary Γ_p, i.e.,

$$(6.5) \qquad \boldsymbol{\sigma}_p \boldsymbol{n}_p = \rho_p c_{pI}(\partial_t \boldsymbol{u}_p \cdot \boldsymbol{n}_p)\boldsymbol{n}_p + \rho_f c_{pII}(\partial_t \boldsymbol{u}_f \cdot \boldsymbol{n}_p)\boldsymbol{n}_p$$
$$+ (\rho_p - \rho_f \phi/a)c_s(I - \boldsymbol{n}_p \boldsymbol{n}_p) \cdot \partial_t \boldsymbol{u}_p,$$
$$-p\boldsymbol{n}_p = \rho_f a/\phi c_{pII}(\partial_t \boldsymbol{u}_f \cdot \boldsymbol{n}_p)\boldsymbol{n}_p + \rho_f c_{pI}(\partial_t \boldsymbol{u}_p \cdot \boldsymbol{n}_p)\boldsymbol{n}_p.$$

In (6.4) $c_p = \sqrt{\frac{\lambda + 2\mu}{\rho_e}}$ and $c_s = \sqrt{\frac{\mu}{\rho_e}}$ are the compressional and shear wave velocities, respectively, while in (6.5) c_{pI} and c_{pII} are the fast and slow compressional wave velocities, respectively, defined as $c_{pI} = \max \sqrt{\Lambda}$ and $c_{pII} = \min \sqrt{\Lambda}$, where Λ are the solutions of the generalized eigenvalue problem $A\boldsymbol{v} = \Lambda B\boldsymbol{v}$ where

$$A = \begin{bmatrix} \rho_p & \rho_f \\ \rho_f & \rho_w \end{bmatrix}, \quad B = \begin{bmatrix} \lambda + 2\mu + m\beta^2 & m\beta \\ m\beta & m \end{bmatrix}.$$

In Figure 7, we report some snapshots of the vertical component velocity $(\dot{\boldsymbol{u}}_p, \dot{\boldsymbol{u}}_e)_y$ obtained by neglecting or considering viscous effects in the model. In particular, we consider the model TC_1 where $\eta = \zeta = 0$ (Figure 7-first row), and the model TC_2 where we set $\eta = 0.0015$ and $\zeta = 0.01$ (Figure 7-second row). The results of TC_1 are in agreement with the ones presented in [60, 62]. Indeed, from Figure 7 (first row), we clearly observe: (i) the continuity of the velocity field across the interface $\Gamma_I = (0, 4800)$ $m \times \{2400\}$ m; (ii) the propagation of the direct fast c_{pI} compressional wave (first front), the reflected fast c_{pI} compressional wave (second front), the reflected shear c_s (third front) and slow compressional c_{pII} wave (fourth front) in the upper poroelastic layer; (iii) the transmitted compressional c_p and shear c_s wave in the lower elastic layer. The same physical phenomena, although less evident, are present when the viscous damping terms are introduced in TC_2, cf. Figure 7(second row). In this case, the transmitted shear c_s and the reflected slow longitudinal c_{PII} waves are too weak to be visible at this scale. From the plot, we can also see the effect of the first-order absorbing boundaries, which are not perfectly transparent. Recent studies have adopted the more efficient perfectly matched layer (PML) methodology, e.g. [56, 49]. The PML implementation is not included in this paper but it will be addressed in the next future.

In Figure 8 we compare the the time histories velocities $(\dot{\boldsymbol{u}}_p, \dot{\boldsymbol{u}}_e)$ at the two receivers $\boldsymbol{x}_{r1} = (2000, 2934)$ m and at $\boldsymbol{x}_{r2} = (2000, 1867)$ m for the different modeling assumptions. Again here we notice the effect of the damping assumption on the scattered wave field.

6.3. Wave propagation in an elastic domain with poroelastic inclusions.
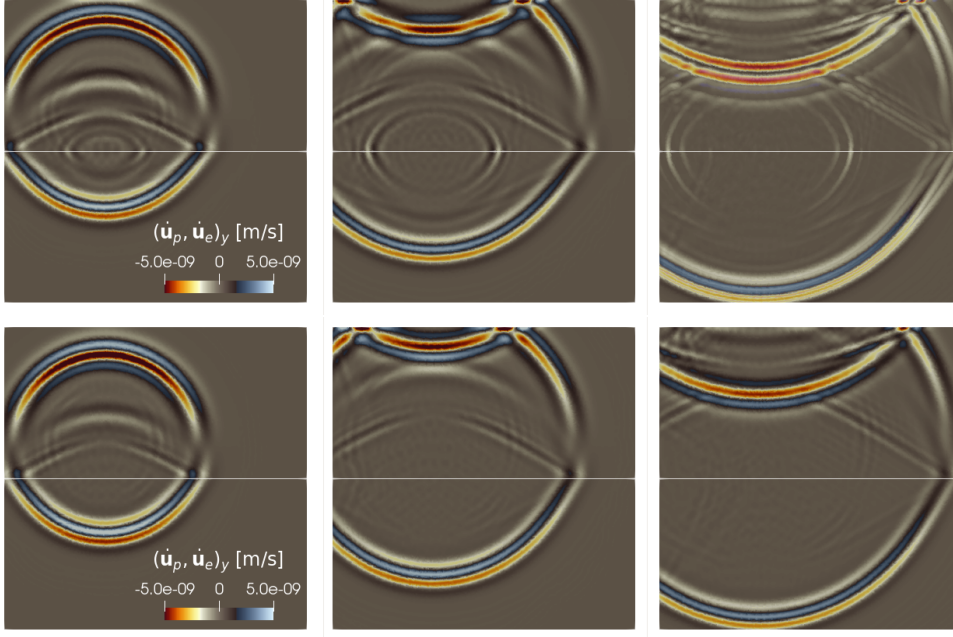To demonstrate the feasibility of tackling a more complex model with the proposed

Fig. 7: Test case of Section 6.2. Snapshots of the vertical component velocity $(\dot{\boldsymbol{u}}_p, \dot{\boldsymbol{u}}_e)_y$ at different time instants: $t = 0.9s$ (left), $t = 1.2s$ (center), and $t = 1.5s$ (right). The top and bottom rows refer to the model TC_1 and TC_2, respectively.
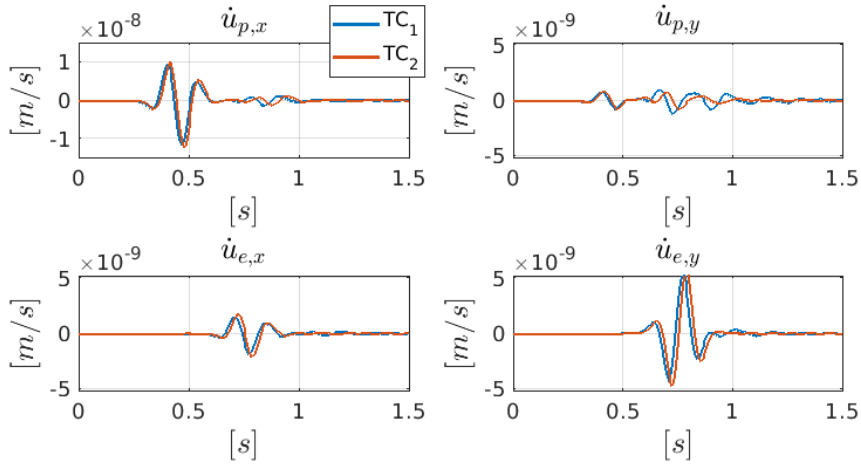

Fig. 8: Test case of Section 6.2. Horizontal and vertical component velocity $\dot{\boldsymbol{u}}_p$ (top) and $\dot{\boldsymbol{u}}_e$ (bottom) for the receivers $\boldsymbol{x}_{r1}$ (top) and $\boldsymbol{x}_{r2}$ (bottom), respectively.

method, we consider a coupled elastic-poroelastic model shown in Figure 6 (right). The background media is regarded as a perfectly elastic medium (whose mechanical properties are listed in Table 3) while the circle and ellipses with different sizes rep-
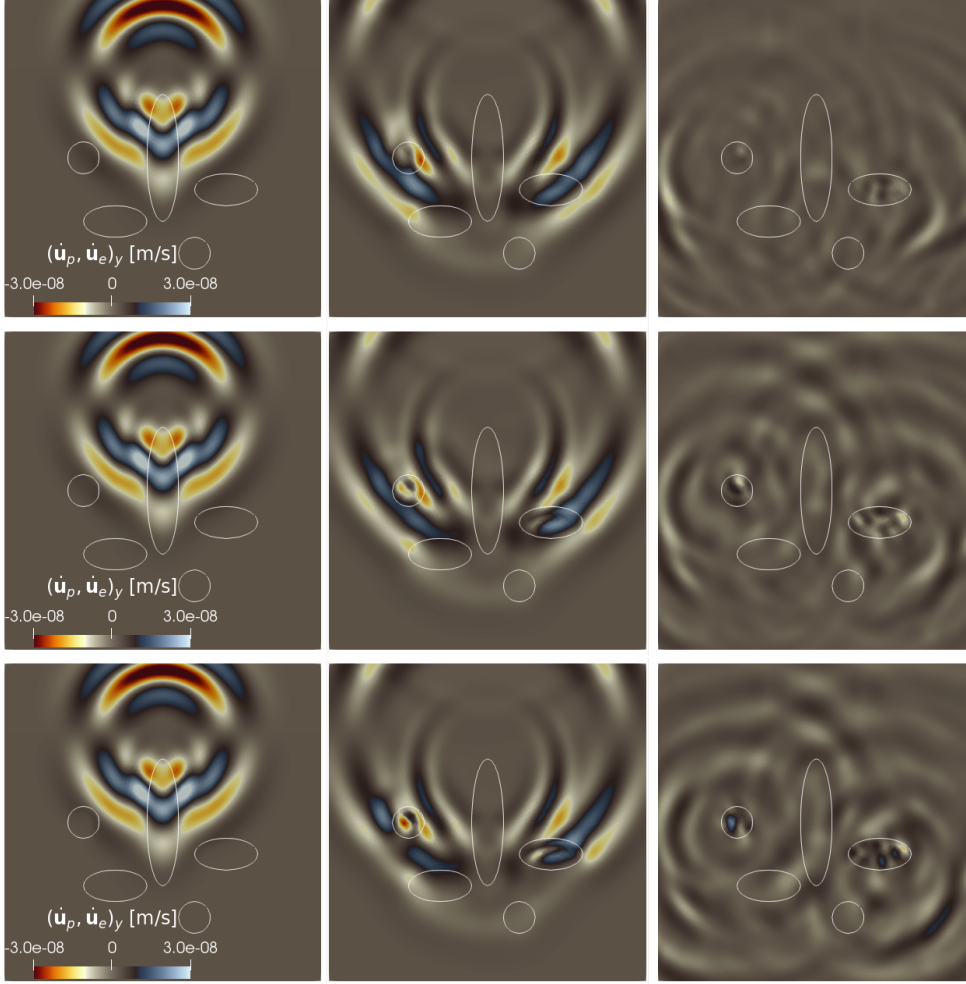
["

Fig. 9: Test case of Section 6.3. Snapshots of the vertical component velocity $(\dot{\boldsymbol{u}}_p, \dot{\boldsymbol{u}}_e)_y$ at different time instants: from left to right $t = 0.3, 0.4, 0.7 \ s$; top row $\delta = 1$, middle row $\delta = 0.5$, bottom row $\delta = 0$.

displacement weak formulation of the problem, we proved stability and error bound for the semi-discretization, where (an interior penalty type) PolydGdG method is considered. Time integration is achieved by an unconditionally stable and implicit dG scheme, which also guarantees high-order accuracy in the time domain. Numerical experiments have been designed not only to verify the numerical performance of the space-time PolydG method but also to exploit the flexibility in the process of mesh design offered by polytopic elements. In this respect, numerical tests of geophysical interest have been also discussed. The presented space-time PolydG method allows a robust and flexible numerical discretization that can be successfully applied to multiphysics wave propagation problems. Future developments in this direction include the extension to realistic three-dimensional problems, the coupling of this model to fluid-structure (with poroelastic, thermo-elastic, or acoustic structure) interaction

problems as well as the design of efficient solvers for the solution of the (linear) system of equations stemming from this space-time PolydG discretization.

Appendix A. Definition of the coupling bilinear form. The aim of this appendix is to motivate the definition of $\mathcal{C}_h(\cdot, \cdot)$ adopted in Section 3.1. We consider equations (2.1) and (2.2), and we multiply them by test functions $\boldsymbol{w}_e \in \boldsymbol{V}_h^e$ and $\boldsymbol{w}_p, \boldsymbol{w}_f \in \boldsymbol{V}_h^p$, respectively, integrate by parts element-wise and focus only to the interface terms, i.e., integrals on Γ_I, namely,

$$
\begin{aligned}
\sum_{i=1}^{5} T_i = &-\int_{\Gamma_I} \boldsymbol{\sigma}_e(\boldsymbol{u}_e)\boldsymbol{n}_e \cdot \boldsymbol{w}_e \, ds - \int_{\Gamma_I} \boldsymbol{\sigma}_e(\boldsymbol{u}_p)\boldsymbol{n}_p \cdot \boldsymbol{w}_p \, ds \\
&+ \delta \int_{\Gamma_I} \beta p(\boldsymbol{u}_p, \boldsymbol{u}_f)\boldsymbol{w}_p \cdot \boldsymbol{n}_p \, ds + (1-\delta) \int_{\Gamma_I} \beta p(\boldsymbol{u}_p, \boldsymbol{u}_f)\boldsymbol{w}_p \cdot \boldsymbol{n}_p \, ds \\
&+ \int_{\Gamma_I} p(\boldsymbol{u}_p, \boldsymbol{u}_f)\boldsymbol{w}_f \cdot \boldsymbol{n}_p \, ds,
\end{aligned}
$$

removing the subscript h to ease the notation. Next, we notice that, in view of condition (2.4), the terms $T_1 + T_2 + T_3$ can be rewritten as

$$
(A.1) \qquad\qquad T_1 + T_2 + T_3 = -\int_{\Gamma_I} \boldsymbol{\sigma}_e(\boldsymbol{u}_e)\boldsymbol{n}_p \cdot (\boldsymbol{w}_p - \boldsymbol{w}_e) \, ds,
$$

while $T_4 + T_5$ as

$$
(A.2) \qquad T_4 + T_5 = -\int_{\Gamma_I} m\nabla \cdot (\beta\boldsymbol{u}_p + \boldsymbol{u}_f)((1-\delta)\beta\boldsymbol{w}_p + \boldsymbol{w}_f) \cdot \boldsymbol{n}_p \, ds.
$$

Then, we add to (A.1) and (A.2) the following strongly consistent terms to ensure the symmetry and positivity of the resulting system:

$$
(A.3) \qquad -\int_{\Gamma_I} \boldsymbol{\sigma}_e(\boldsymbol{v}_e)\boldsymbol{n}_p \cdot (\boldsymbol{u}_p - \boldsymbol{u}_e) \, ds + \int_{\Gamma_I} \alpha(\boldsymbol{u}_p - \boldsymbol{u}_e) \cdot (\boldsymbol{v}_p - \boldsymbol{v}_e) \, ds,
$$

and

$$
(A.4) \quad -\int_{\Gamma_I} m\nabla \cdot (\beta\boldsymbol{w}_p + \boldsymbol{w}_f)((1-\delta)\beta\boldsymbol{u}_p + \boldsymbol{u}_f) \cdot \boldsymbol{n}_p \, ds
$$

$$
+ \gamma \int_{\Gamma_I} ((1-\delta)\beta\boldsymbol{u}_p + \boldsymbol{u}_f) \cdot \boldsymbol{n}_p((1-\delta)\beta\boldsymbol{v}_p + \boldsymbol{v}_f) \cdot \boldsymbol{n}_p \, ds,
$$

being α and γ defined as in (3.5)–(3.6). Finally, summing up equations (A.1)–(A.4) we get

$$
\begin{aligned}
\mathcal{C}_h(\mathsf{U}, \mathsf{W}) = &-\langle \boldsymbol{\sigma}_e(\boldsymbol{u}_e)\boldsymbol{n}_p, \boldsymbol{w}_p - \boldsymbol{w}_e \rangle_{\mathcal{F}_h^I} - \langle \boldsymbol{\sigma}_e(\boldsymbol{v}_e)\boldsymbol{n}_p, \boldsymbol{u}_p - \boldsymbol{u}_e \rangle_{\mathcal{F}_h^I} + \langle \alpha\boldsymbol{u}_p - \boldsymbol{u}_e, \boldsymbol{v}_p - \boldsymbol{v}_e \rangle_{\mathcal{F}_h^I} \\
&- \langle m\nabla \cdot (\beta\boldsymbol{u}_p + \boldsymbol{u}_f), ((1-\delta)\beta\boldsymbol{w}_p + \boldsymbol{w}_f) \cdot \boldsymbol{n}_p \rangle_{\Gamma_I} \\
&- \langle m\nabla \cdot (\beta\boldsymbol{w}_p + \boldsymbol{w}_f), ((1-\delta)\beta\boldsymbol{u}_p + \boldsymbol{u}_f) \cdot \boldsymbol{n}_p \rangle_{\mathcal{F}_h^I} \\
&+ \gamma\langle ((1-\delta)\beta\boldsymbol{u}_p + \boldsymbol{u}_f) \cdot \boldsymbol{n}_p, ((1-\delta)\beta\boldsymbol{v}_p + \boldsymbol{v}_f) \cdot \boldsymbol{n}_p \rangle_{\mathcal{F}_h^I},
\end{aligned}
$$

that is definition (3.7). Note that $\mathcal{C}_h(\mathsf{U}, \mathsf{W}) = \mathcal{C}_h(\mathsf{W}, \mathsf{U})$.

References.

[1] R. ABEDI, B. PETRACOVICI, AND R. B. HABER, *A space–time discontinuous Galerkin method for linearized elastodynamics with element-wise momentum balance*, Computer Methods in Applied Mechanics and Engineering, 195 (2006), pp. 3247–3273.

[2] C. AGUT AND J. DIAZ, *Stability analysis of the Interior Penalty Discontinuous Galerkin method for the wave equation*, ESAIM: Mathematical Modelling and Numerical Analysis - Modélisation Mathématique et Analyse Numérique, 47 (2013), pp. 903–932.

[3] I. AMBARTSUMYAN, E. KHATTATOV, I. YOTOV, AND P. ZUNINO, *A Lagrange multiplier method for a Stokes–Biot fluid–poroelastic structure interaction model*, Numerische Mathematik, 140 (2018), pp. 513–553.

[4] V. ANAYA, Z. DE WIJN, B. GÓMEZ-VARGAS, D. MORA, AND R. RUIZ-BAIER, *Rotation-based mixed formulations for an elasticity-poroelasticity interface problem*, SIAM Journal on Scientific Computing, 42 (2020), pp. B225–B249.

[5] P. F. ANTONIETTI, F. BONALDI, AND I. MAZZIERI, *A high-order discontinuous Galerkin approach to the elasto-acoustic problem*, Comput. Methods Appl. Mech. Engrg., 358 (2020), pp. 112634, 29.

[6] P. F. ANTONIETTI, F. BONALDI, AND I. MAZZIERI, *Simulation of three-dimensional elastoacoustic wave propagation based on a Discontinuous Galerkin Spectral Element Method*, Internat. J. Numer. Methods Engrg., 121 (2020), pp. 2206–2226.

[7] P. F. ANTONIETTI, S. BONETTI, AND M. BOTTI, *Discontinuous galerkin approximation of the fully coupled thermo-poroelastic problem*, SIAM Journal on Scientific Computing, 45 (2023), pp. A621–A645.

[8] P. F. ANTONIETTI, M. BOTTI, AND I. MAZZIERI, *On mathematical and numerical modelling of multiphysics wave propagation with polytopal discontinuous Galerkin methods: a review*, Vietnam Journal of Mathematics, (2022), pp. 1–32.

[9] P. F. ANTONIETTI, M. BOTTI, I. MAZZIERI, AND S. N. POLTRI, *A high-order discontinuous galerkin method for the poro-elasto-acoustic problem on polygonal and polyhedral grids*, SIAM Journal on Scientific Computing, 44 (2022), pp. B1–B28.

[10] P. F. ANTONIETTI, F. BREZZI, AND L. D. MARINI, *Bubble stabilization of discontinuous galerkin methods*, Comput. Methods Appl. Mech. Engrg., 198 (2009), pp. 1651–1659.

[11] P. F. ANTONIETTI, N. DAL SANTO, I. MAZZIERI, AND A. QUARTERONI, *A high-order discontinuous Galerkin approximation to ordinary differential equations with applications to elastodynamics*, IMA Journal of Numerical Analysis, 38 (2018), pp. 1709–1734.

[12] P. F. ANTONIETTI, S. GIANI, AND P. HOUSTON, *hp-version composite Discontinuous Galerkin methods for elliptic problems on complicated domains*, SIAM J. Sci. Comput., 35 (2013), pp. A1417–A1439.

[13] P. F. ANTONIETTI AND I. MAZZIERI, *High-order discontinuous Galerkin methods for the elastodynamics equation on polygonal and polyhedral meshes*, Comput. Methods Appl. Mech. Engrg., 342 (2018), pp. 414–437.

[14] P. F. ANTONIETTI, I. MAZZIERI, AND F. MIGLIORINI, *A discontinuous Galerkin time integration scheme for second order differential equations with applications to seismic wave propagation problems*, Computers and Mathematics with Applications, 134 (2023), pp. 87–100.

[15] P. F. ANTONIETTI, I. MAZZIERI, M. MUHR, V. NIKOLIĆ, AND B. WOHLMUTH, *A high-order discontinuous Galerkin method for nonlinear sound waves*, J. Com-

put phys, 415 (2020), p. 109484.

[16] D. N. ARNOLD, F. BREZZI, B. COCKBURN, AND L. D. MARINI, *Unified analysis of discontinuous Galerkin methods for elliptic problems*, SIAM Journal on Numerical Analysis, 39 (2001/02), pp. 1749–1779.

[17] H. T. BANKS, M. J. BIRCH, M. P. BREWIN, S. E. GREENWALD, S. HU, Z. R. KENZ, C. KRUSE, M. MAISCHAK, S. SHAW, AND J. R. WHITEMAN, *High-order space-time finite element schemes for acoustic and viscodynamic wave equations with temporal decoupling*, International Journal for Numerical Methods in Engineering, 98 (2014), pp. 131–156.

[18] H. BARUCQ, H. CALANDRA, J. DIAZ, AND E. SHISHENINA, *Space–time Trefftz-dg approximation for elasto-acoustics*, Applicable Analysis, 99 (2018), pp. 747–760.

[19] F. BASSI, L. BOTTI, A. COLOMBO, D. A. DI PIETRO, AND P. TESINI, *On the flexibility of agglomeration based physical space discontinuous Galerkin discretizations*, J. Comput. Phys., 231 (2012), pp. 45–65.

[20] M. BAUSE, F. A. RADU, AND U. KÖCHER, *Space–time finite element approximation of the biot poroelasticity system with iterative coupling*, Computer Methods in Applied Mechanics and Engineering, 320 (2017), pp. 745–768.

[21] A. BERMÙDEZ, R. RODRÌGUEZ, AND D. SANTAMARINA, *Finite element approximation of a displacement formulation for time-domain elastoacoustic vibrations*, Journal of Computational and Applied Mathematics, 152 (2003), pp. 17 – 34.

[22] M. A. BIOT, *Theory of elasticity and consolidation for a porous anisotropic solid*, Journal of applied physics, 26 (1955), pp. 182–185.

[23] S. BONETTI, M. BOTTI, I. MAZZIERI, AND P. F. ANTONIETTI, *Numerical modelling of wave propagation phenomena in thermo-poroelastic media via discontinuous galerkin methods*, 2023, https://arxiv.org/abs/2303.09481.

[24] R. BÜRGER, S. KUMAR, D. MORA, R. RUIZ-BAIER, AND N. VERMA, *Virtual element methods for the three-field formulation of time-dependent linear poroelasticity*, Advances in Computational Mathematics, 47 (2021), pp. 1–37.

[25] J. BUTCHER, *Runge–Kutta Methods*, John Wiley & Sons, Ltd, 2016, ch. 3, pp. 143–331.

[26] A. CANGIANI, Z. DONG, AND E. GEORGOULIS, *hp-version discontinuous galerkin methods on essentially arbitrarily-shaped elements*, Mathematics of Computation, 91 (2022), pp. 1–35.

[27] A. CANGIANI, Z. DONG, AND E. H. GEORGOULIS, *hp-version space-time discontinuous Galerkin methods for parabolic problems on prismatic meshes*, SIAM J. Sci. Comput., 39 (2017), pp. A1251–A1279.

[28] A. CANGIANI, Z. DONG, E. H. GEORGOULIS, AND P. HOUSTON, *hp-version discontinuous Galerkin methods for advection-diffusion-reaction problems on polytopic meshes*, ESAIM Math. Model. Numer. Anal., 50 (2016), pp. 699–725.

[29] A. CANGIANI, Z. DONG, E. H. GEORGOULIS, AND P. HOUSTON, *hp-version discontinuous Galerkin methods on polytopic meshes*, SpringerBriefs in Mathematics, Springer International Publishing, 2017.

[30] A. CANGIANI, E. H. GEORGOULIS, AND P. HOUSTON, *hp-version discontinuous Galerkin methods on polygonal and polyhedral meshes*, Mathematical Models and Methods in Applied Sciences, 24 (2014), pp. 2009–2041.

[31] J. CARCIONE, *Wave Fields in Real Media*, vol. 38, Elsevier Science, 2014.

[32] B. CASTAGNEDE, A. AKNINE, M. MELON, AND C. DEPOLLIER, *Ultrasonic characterization of the anisotropic behavior of air-saturated porous materials*, Ultrasonics, 36 (1998), pp. 323–341.

[33] G. Chiavassa and B. Lombard, *Wave propagation across acoustic/Biot's media: A finite-difference method*, Communications in Computational Physics, 13 (2013), pp. 985–1012.

[34] S. Congreve and P. Houston, *Two-grid hp-DGFEMs on agglomerated coarse meshes*, PAMM, 19 (2019), p. e201900175.

[35] N. Dai, A. Vafidis, and E. Kanasewich, *Wave propagation in heterogeneous, porous media; a velocity-stress, finite-difference method*, Geophysics, 60 (1995), pp. 327–340.

[36] J. de la Puente, M. Dumbser, M. Käser, and H. Igel, *Discontinuous Galerkin methods for wave propagation in poroelastic media*, Geophysics, 73 (2008), pp. T77–T97.

[37] M. Delfour, W. Hager, and F. Trochu, *Discontinuous Galerkin methods for ordinary differential equations*, Mathematics of Computation, 36 (1981), pp. 455–473.

[38] W. Dörfler, S. Findeisen, and C. Wieners, *Space-time discontinuous Galerkin discretizations for linear first-order hyperbolic evolution systems*, Computer Methods in Applied Mathematics, 16 (2016), pp. 409–428.

[39] B. Dupuy, L. De Barros, S. Garambois, and J. Virieux, *Wave propagation in heterogeneous porous media formulated in the frequency-space domain using a discontinuous galerkin method*, Geophysics, 76 (2011), pp. N13–N28.

[40] A. Ezziani, *Modélisation mathématique et numérique de la propagation d'ondes dans les milieux viscoélastiques et poroélastiques*, theses, ENSTA ParisTech, 2005, https://pastel.archives-ouvertes.fr/tel-00009179.

[41] M. Ferro and W. Mansur, *Wave propagation in elastic and poroelastic media in the frequency domain by the boundary element method*, in 28th World conference on boundary elements and other mesh reduction methods. WIT transactions on modelling and simulation, vol. 42, 2006, pp. 285–293.

[42] B. Flemisch, M. Kaltenbacher, S. Triebenbacher, and B. Wohlmuth, *The equivalence of standard and mixed finite element methods in applications to elasto-acoustic interaction*, SIAM J. Sci. Comput., 32 (2010), p. 1980–2006.

[43] B. Flemisch, M. Kaltenbacher, and B. Wohlmuth, *Elasto-acoustic and acoustic-acoustic coupling on non-matching grids*, Internat. J. Numer. Methods Engrg., 67 (2006), pp. 1791–1810.

[44] D. A. French, *A space-time finite element method for the wave equation*, Computer Methods in Applied Mechanics and Engineering, 107 (1993), pp. 145 – 157.

[45] V. Girault, G. Pencheva, M. Wheeler, and T. Wildey, *Domain decomposition for poroelasticity and elasticity with dg jumps and mortars*, Mathematical Models and Methods in Applied Sciences, 21 (2011), pp. 169–213.

[46] J. Gopalakrishnan, J. Schöberl, and C. Wintersteiger, *Mapped tent pitching schemes for hyperbolic systems*, Computational Methods in Science and Engineering, 39 (2017), pp. B1043–B1063.

[47] D. Gregor, P. Moczo, J. Kristek, A. Mesgouez, G. Lefeuve-Mesgouez, C. Morency, J. Diaz, and M. Kristekova, *Seismic waves in medium with poroelastic/elastic interfaces: a two-dimensional P-SV finite-difference modelling*, Geophysical Journal International, 228 (2021), pp. 551–588.

[48] T. Haire and C. Langton, *Biot theory: a review of its application to ultrasound propagation through cancellous bone*, Bone, 24 (1999), pp. 291 – 295.

[49] Y. He, T. Chen, and J. Gao, *Unsplit perfectly matched layer absorbing boundary conditions for second-order poroelastic wave equations*, Wave Motion, 89

(2019), pp. 116–130.

[50] T. HUGHES AND G. HULBERT, *Space-time finite element methods for elastodynamics: formulation and error estimates*, Computer Methods in Applied Mechanics and Engineering, 66 (1988), pp. 339–363.

[51] L. O. JAY, *Lobatto Methods*, Springer Berlin Heidelberg, Berlin, Heidelberg, 2015, pp. 817–826.

[52] C. JOHNSON, *Discontinuous Galerkin finite element methods for second order hyperbolic problems*, Computer Methods in Applied Mechanics and Engineering, 107 (1993), pp. 117 – 129.

[53] F. KRETZSCHMAR, A. MOIOLA, I. PERUGIA, AND S. M. SCHENPP, *A priori error analysis of space-time Trefftz discontinuous Galerkin methods for wave problems*, IMA Journal of Numerical Analysis, 36 (2016), pp. 1599–1635.

[54] B. KRISHNAN, D. M., S. RAJA, AND K. VENKATARAMANA, *Structural and Vibroacoustic Analysis of Aircraft Fuselage Section with Passive Noise Reducing Materials: A Material Performance Study*, in 4th International Engineering Symposium, 03 2015.

[55] G. LEFEUVE-MESGOUEZ, A. MESGOUEZ, G. CHIAVASSA, AND B. LOMBARD, *Semi-analytical and numerical methods for computing transient waves in 2d acoustic/poroelastic stratified media*, Wave Motion, 49 (2012), pp. 667–680.

[56] R. MARTIN, D. KOMATITSCH, AND A. EZZIANI, *An unsplit convolutional perfectly matched layer improved at grazing incidence for seismic wave propagation in poroelastic media*, Geophysics, 73 (2008), pp. T51–T61.

[57] Y. J. MASSON AND S. R. PRIDE, *Finite-difference modeling of biot's poroelastic equations across all frequencies*, Geophysics, 75 (2010), pp. N33–N41.

[58] A. MOIOLA AND I. PERUGIA, *A space–time Trefftz discontinuous Galerkin method for the acoustic wave equation in first-order formulation*, Numerische Mathematik, 138 (2018), pp. 389–435.

[59] C. MORENCY, Y. LUO, AND J. TROMP, *Acoustic, elastic and poroelastic simulations of CO2 sequestration crosswell monitoring based on spectral-element and adjoint methods*, Geophysical Journal International, 185 (2011), pp. 955–966.

[60] C. MORENCY AND J. TROMP, *Spectral-element simulations of wave propagation in porous media*, Geophysical Journal International, 175 (2008), pp. 301–345.

[61] R. H. NOCHETTO, S. A. SAUTER, AND C. WIENERS, *Space-time methods for time-dependent partial differential equations*, Oberwolfach Reports, 14 (2018), pp. 863–947.

[62] H. PENG, Y. SRIPANICH, I. VASCONCELOS, AND J. TRAMPERT, *Benchmarking wave equation solvers using interface conditions: the case of porous media*, Geophysical Journal International, 224 (2020), pp. 355–376.

[63] H. PENG, Y. SRIPANICH, I. VASCONCELOS, AND J. TRAMPERT, *Benchmarking wave equation solvers using interface conditions: the case of porous media*, Geophysical Journal International, 224 (2021), pp. 355–376.

[64] I. PERUGIA, J. SCHÖBERL, P. STOCKER, AND C. WINTERSTEIGER, *Tent pitching and Trefftz-dg method for the acoustic wave equation*, Computers & Mathematics with Applications, 79 (2020), pp. 2987–3000.

[65] P. J. PHILLIPS AND M. F. WHEELER, *A coupling of mixed and discontinuous galerkin finite-element methods for poroelasticity*, Computational Geosciences, 12 (2008), pp. 417–435.

[66] A. QUARTERONI, R. SACCO, AND F. SALERI, *Numerical Mathematics*, vol. 2, Springer Berlin, Heidelberg, 2007.

[67] R. T. ROCKAFELLAR, *Lagrange multipliers and optimality*, SIAM review, 35

(1993), pp. 183–238.

[68] R. Sidler, J. M. Carcione, and K. Holliger, *Simulation of surface waves in porous media*, Geophysical Journal International, 183 (2010), pp. 820–832.

[69] B. S. Southworth, O. Krzysik, W. Pazner, and H. D. Sterck, *Fast solution of fully implicit runge–kutta and discontinuous galerkin in time for numerical pdes, part i: the linear setting*, SIAM Journal on Scientific Computing, 44 (2022), pp. A416–A443.

[70] M. Souzanchi, L. Cardoso, and S. Cowin, *Tortuosity and the averaging of microvelocity fields in poroelasticity*, Journal of applied mechanics, 80 (2013).

[71] R. Stacey, *Improved transparent boundary formulations for the elastic-wave equation*, Bulletin of the Seismological Society of America, 78 (1988), pp. 2089–2097.

[72] E. M. Stein, *Singular integrals and differentiability properties of functions*, vol. 2, Princeton University Press, 1970.

[73] S. Triebenbacher, M. Kaltenbacher, B. Wohlmuth, and B. Flemisch, *Applications of the mortar finite element method in vibroacoustics and flow induced noise computations*, Acta Acustica united with Acustica, 96 (2010), pp. 536–553(18).

[74] J. van der Vegt, C. Klaji, F. van der Bos, and H. van der Ven, *Space-time discontinuous Galerkin method for the compressible navier-stokes equations on deforming meshes*, European Conference on Computational Fluid Dynamics ECCOMAS CFD 2006, (2006).

[75] A. K. Vashisth, M. D. Sharma, and M. L. Gogna, *Reflection and transmission of elastic waves at a loosely bonded interface between an elastic solid and liquid-saturated porous solid*, Geophysical Journal International, 105 (1991), pp. 601–617.

[76] N. D. Ward, T. Lähivaara, and S. Eveson, *A discontinuous galerkin method for poroelastic wave propagation: The two-dimensional case*, Journal of Computational Physics, 350 (2017), pp. 690–727.

[77] F. Wenzlau and T. M. Müller, *Finite-difference modeling of wave propagation and diffusion in poroelastic media*, Geophysics, 74 (2009), pp. T55–T66.

[78] Q. Zhan, M. Zhuang, Y. Mao, and Q. H. Liu, *Unified riemann solution for multi-physics coupling: Anisotropic poroelastic/elastic/fluid interfaces*, Journal of Computational Physics, 402 (2020), p. 108961.

[79] Y. Zhang and J. Gao, *A 3d staggered-grid finite difference scheme for poroelastic wave equation*, Journal of Applied Geophysics, 109 (2014), pp. 281–291.

[80] Y. Zhang, J. Gao, W. Han, and Y. He, *A discontinuous galerkin method for seismic wave propagation in coupled elastic and poroelastic media*, Geophysical Prospecting, 67 (2019), pp. 1392–1403.

[81] Y. Zhang, J. Gao, W. Han, and Y. He, *A discontinuous galerkin method for seismic wave propagation in coupled elastic and poroelastic media*, Geophysical Prospecting, 67 (2019), pp. 1392–1403.

MOX Technical Reports, last issues

51/2023   Bucelli, M.; Regazzoni, F.; Dede', L.; Quarteroni, A.

Preserving the positivity of the deformation gradient determinant in intergrid interpolation by combining RBFs and SVD: application to cardiac electromechanics

49/2023   Ieva, F.; Ronzulli, M.; Romo, J.; Paganoni, A.M.

A Spearman Dependence Matrix for Multivariate Functional Data

48/2023   Renzi, F.; Vergara, C.; Fedele, M.; Giambruno, V.; Quarteroni, A.; Puppini, G.; Luciani, G.B.

Accurate and Efficient 3D Reconstruction of Right Heart Shape and Motion from Multi-Series Cine-MRI

45/2023   Gironi, P.; Petraro, L.; Santoni, S.; Dede', L.; Colosimo, B.M.

A Computational Model of Cell Viability and Proliferation of Extrusion-based 3D Bioprinted Constructs During Tissue Maturation Process

44/2023   Fontana, N.; Savaré, L.; Rea, F.; Di Angelantonio, E.; Ieva, F.

Long-term adherence to polytherapy in heart failure patients: a novel approach emphasising the importance of secondary prevention

42/2023   Tonini, A.; Vergara, C.; Regazzoni, F.; Dedè, L.; Scrofani, R.; Cogliati, C.; Quarteroni, A.

A mathematical model to assess the effects of COVID-19 on the cardiocirculatory system

41/2023   Corti M.; Bonizzoni, F.; Antonietti, P.F.; Quarteroni, A.M.

Uncertainty Quantification for Fisher-Kolmogorov Equation on Graphs with Application to Patient-Specific Alzheimer Disease

40/2023   Ballini, E.; Chiappa, A.S.; Micheletti, S.

Reducing the Drag of a Bluff Body by Deep Reinforcement Learning

39/2023   Riccobelli, D.; Al-Terke, H. H.; Laaksonen, P.; Metrangolo, P.; Paananen, A.; Ras, R. H. A.; Ciarletta, P.; Vella, D.

Flattened and wrinkled encapsulated droplets: Shape-morphing induced by gravity and evaporation

37/2023   Regazzoni, F.; Pagani, S.; Salvador, M.; Dede', L.; Quarteroni, A.

Latent Dynamics Networks (LDNets): learning the intrinsic dynamics of spatio-temporal processes